Spring 5-15-2023

Spike-Timing-Dependent Plasticity Alters Sensory Network Connectivity

Adalee Lube

WASHINGTON UNIVERSITY IN SAINT LOUIS

Division of Biology and Biomedical Sciences
Neuroscience

Dissertation Examination Committee:
Bruce A. Carlson, Chair
Martha Bagnall
Keith Hengen
Steve Mennerick
Barani Raman

Spike-Timing-Dependent Plasticity Alters Sensory Network Connectivity

by
Adalee Jeannine Lube

A dissertation presented to

Washington University in St. Louis

in partial fulfillment of the

requirements for the degree

of Doctor of Philosophy

May 2023
Saint Louis, Missouri

TABLE OF CONTENTS

LIST OF FIGURES

LIST OF TABLES

ACKNOWLEDGEMENTS

Firstly, I would like to thank Bruce Carlson, my advisor, for his mentorship and support for the past seven years. I've learned so much about how to be a better scientist from his guidance. His encouragement for not only my PhD education, but also my future career, allowed me to develop my skills both as a scientist and a teaching instructor throughout my time in graduate school. His mentorship style and understanding of people attracts the best scientists, and best people, to the lab which fosters an incredible lab community.

I also want to acknowledge the members of my thesis committee: Steve Mennerick, Martha Bagnall, Barani Raman, and Keith Hengen. If I were to properly acknowledge how each member individually and as a group contributed to my development as scientist, it would take up multiple pages. So instead, I will thank all of them for their enthusiasm, mentorship, and understanding concerning my thesis. Their ideas were integral to the development and success of this project.

I would also like to thank other Biology Department faculty and staff who have helped me grow as a scientist. In the summer of 2012, before I started undergrad at Wash U, I spent a summer in Yehuda Ben-Shahar's lab. I felt so inspired, valued, and intellectually stimulated that I decided to go to grad school. As I stayed at Wash U for my PhD education, Yehuda was still an integral part of my growth as a scientist. I also wanted to thank Mary Lambo, Elise Walck-Shannon, and Mitch Kundel for contributing to my development as an educator. Once I realized I wanted to be a university lecturer, they all allowed me to contribute to the classes I TA'd with them in meaningful ways so I could grow as a lecturer.

I would like to thank my colleagues in the Carlson Lab for their advice, support, and friendship throughout my graduate school education: Alejandro Vélez, Kim Sukhum, Erika

Schumacher, Matasaburo Fukutomi, Marty Jarzyna, and Ellen Urquhart. I wanted to especially thank Erika Schumacher, who went on this PhD journey with me, for her incredible friendship and support. I could not have done it without her. I also wanted to thank former Carlson lab post-doc Xiaofeng Ma, whose work *in vitro* led to the questions that motivated this thesis. Further, this work would not have been possible without the many undergraduates that I've had the privilege to mentor including Amelia Mitchell, Jadey Sadoff, and Justin Fong.

I would like to thank the Neuroscience graduate students for being a wonderful and supportive community. I'd like to particularly thank Ryan Raut, Stephanie Schultz, Melvin King, Lorenzo Lones, Saul Bello-Rojas, Allison Soung and Margaret Hayne for being the greatest friend group a grad student could ask for. Graduate school would not have been the same without them.

I would like to thank my friends and family outside of graduate school, especially my parents Lynda and Richard Lube. Their unconditional love and support to pursue my dreams and become whoever I wanted to be is what gave me the confidence to complete a PhD. I would not have completed any of my degrees without them.

Adalee Lube

Washington University in St. Louis

May 2023

ABSTRACT OF DISSERTATION

Spike-Timing-Dependent Plasticity Alters Sensory Network Connectivity

by

Adalee Lube

Doctor of Philosophy in Biology and Biomedical Sciences

Program in Neurosciences

Washington University in St. Louis, 2023

Professor Bruce A. Carlson, Advisor

Professor Steve Mennerick, Chair

A fundamental question in neuroscience is: how does a sensory system optimize detection of behaviorally relevant stimuli, when those stimuli and the sensory environment are constantly changing? Spike-timing-dependent plasticity (STDP), in which synapse strength changes based on the relative timing of pre- and post-synaptic spiking, has been implicated in changes in neuronal connectivity thought to underlie learning and memory. Synaptic strength changes caused by STDP have been shown in optic tectum, visual cortex, hippocampus, and other brain regions *in vitro* across many organisms like fish, frogs, and mice. Although it is possible that STDP mechanisms underlie changes in sensory neuron connectivity, the relationship between sensory stimulation and central sensory neuronal response is complex and often involves populations of neurons that differ in the timing and frequency of spiking, resulting in complex spatiotemporal patterns of synaptic input to postsynaptic neurons. The organism I studied, weakly electric fish, produce and receive electric organ discharges (EODs) used to electrolocate and communicate. Taking advantage of the electrosensory system, weakly electric fishes are a system in which spiking patterns are themselves the behaviorally relevant stimulus. Previous work showed that STDP predictably altered synaptic

responses and inter-pulse interval tuning *in vitro* (Ma and Carlson, unpublished). Using whole-cell intracellular recordings to repetitively pair sensory stimulation with intracellular spiking *in vivo*, I manipulated the relative timing of pre- and post-synaptic spiking in central sensory neurons in awake, behaving animals. I found that STDP alters sensory responses of central electrosensory neurons *in vivo* but there was more variability in the changes in sensory responses *in vivo* relative to the *in vitro* changes in synaptic responses (Chapter 2). Whether the *in vivo* data "fit" or "did not fit" the pattern predicted by the *in vitro* results was correlated with variations in synaptic potential landmarks. That variations in synaptic potential landmarks correlated with deviations from the pattern shown *in vitro* results suggest that whether the data "fit" or "did not fit" the *in vitro* hypothesis is influenced by polysynaptic activity, including inhibitory interneurons (Chapter 2). I now asked whether STDP could alter sensory tuning to behaviorally relevant stimuli *in vivo*. Using whole-cell intracellular recordings, I recorded postsynaptic potential responses to two different sensory stimuli before and after pairing postsynaptic spiking with only one of those sensory stimuli. I found that some *in vivo* responses followed the pattern predicted by STDP sensory tuning experiments done *in vitro* and some *in vivo* responses that did not. Whether the *in vivo* sensory tuning data "fit" or "did not fit" the pattern predicted by the *in vitro* sensory tuning changes was correlated with variations in synaptic potential landmarks. That variations in the synaptic potential landmarks correlated with differences in the *in vitro* and *in vivo* sensory tuning suggest that whether the *in vivo* tuning results did or did not "fit" the *in vitro* tuning prediction is influenced by polysynaptic activity, including inhibitory interneurons (Chapter 3). Next, I wanted to ask whether intrinsic network activity could alter sensory tuning based solely on the input of behaviorally relevant stimuli. Using extracellular evoked potential recordings and a freely behaving paradigm, I recorded postsynaptic potential responses and behavioral output to two

different sensory stimuli before and after repeating only one of those sensory stimuli, with no pairing of postsynaptic spiking. I did not find any significant differences in the evoked potentials or behavior as a result of repetition of a sensory stimulus (Chapter 4). Thus, in this dissertation I showed that STDP can alter the sensory responses of central electrosensory neurons, but that STDP rules operating at identified synapses may not drive predictable changes in sensory responses and sensory tuning at the circuit or behavioral level. In conclusion, for altering sensory tuning in adult organisms in a changing sensory environment *in vivo*, the role of STDP is more complex than had been predicted from previous work *in vitro.*

CHAPTER 1

Introduction

1.1 Introduction

A fundamental problem in neuroscience is how circuits extract behaviorally relevant information coded in spike times. Temporal codes have been implicated in processing within many sensory systems (Bell and Grant, 1989; Gooler and Feng, 1992; Hollrigel et al., 1998; Covey and Casseday, 1999; Xu-Friedman and Hopkins, 1999; Carlson and Kawasaki, 2008; Baker et al., 2013), and previous work has shown mechanisms by which sensory circuits can decode temporal patterns (Carlson and Kawasaki, 2008; Baker et al., 2013, 2016; Baker and Carlson, 2014; Aumentado-Armstrong et al., 2015). However, the sensory environment is always changing. My central question was: How does a sensory system optimize detection of behaviorally relevant stimuli amidst constant changes in those stimuli and to the sensory environment? The adjustment of synaptic connectivity via spike-timing-dependent plasticity (STDP) has been demonstrated in circuits across diverse invertebrate and vertebrate organisms (Dan and Poo, 2004; Feldman, 2012). The importance of STDP in sensory processing and behavior, however, has been explored very little. Pairing sensory stimulation with intracellular spiking can elicit changes in synaptic strength through STDP (Markram et al., 1997; Bi and Poo, 1998; Song et al., 2000). However, since previous STDP experiments have relied on artificially induced postsynaptic spiking via intracellular current injection (Bell et al., 1997; Bi and Poo, 2001; Dan and Poo, 2004; Caporale and Dan, 2008; Feldman, 2012), this does not reveal how STDP alters connections under natural conditions.

Experiments *in vivo* that have delivered two sensory pulses at an appropriate delay have shown neuronal changes in sensory tuning consistent with STDP measured *in vitro* (Froemke and Dan, 2002; Nelken, 2004; Froemke, 2010), although this is only indirect evidence that STDP underlies these changes. The inability of these studies to directly tie *in vitro* induction of STDP to

in vivo neuronal changes prevents understanding of the exact mechanisms that enable sensory tuning *in vivo*. I will take advantage of a system in which presynaptic input can be precisely manipulated with sensory stimulation and behaviorally relevant sensory stimuli can be faithfully replicated. Determining how sensory experience changes neural connectivity is instrumental to understanding how an organism retains flexible tuning as the environment changes, and how it translates sensory experience into behavior. In this thesis, I aim to understand mechanisms that could allow for tuning adaptation in a quickly changing sensory environment.

1.2 Spike-timing-dependent plasticity (STDP)

The adjustment of synaptic connectivity via STDP, wherein synaptic strength is altered based on the relative timing of repetitive pre- and postsynaptic activity, has been demonstrated in sensory circuits across diverse invertebrate and vertebrate organisms(Bell et al., 1997; Markram et al., 1997; Bi and Poo, 1998; Dan and Poo, 2004; Feldman, 2012). *In vitro* studies across many brain regions and organisms reveal that repeated pre-leads postsynaptic spiking induces synaptic potentiation, whereas the reverse timing induces synaptic depression(Markram et al., 1997; Bi and Poo, 1998; Song et al., 2000). In 1997, Markram et al. discovered, in pyramidal neurons, that EPSP amplitude decreased in the neurons in which the postsynaptic action potentials occurred 10 ms before the EPSP, while the EPSP amplitude increased when the postsynaptic action potentials occurred 10 ms after the onset of the EPSP. In 1998, Bi and Poo showed, in hippocampal neurons, that potentiation occurred in a window of pre-leads post synaptic activation by 20 ms or less and that depression occurred in a window of post-leads presynaptic activation by 20 ms or less. In 2000, Song et al. named this phenomenon “spike-timing-dependent plasticity” in a modeling study that showed that STDP could balance synaptic strengths to make postsynaptic firing more sensitive

to presynaptic spike timing and thus, make pre- and postsynaptic spike times causally correlated. Since these initial landmark studies, this Hebbian form of STDP has been explored in both wet lab settings, *in vitro* and *in vivo,* and in computational models that explore many circuits (Song et al., 2000; Morrison et al., 2008; Feldman, 2012; Huang and Wei, 2021).

Neuronal connectivity changes consistent with STDP have been observed in the development of receptive fields (Mu and Poo, 2006; Richards, 2010) and establishment of direction selectivity within the visual system (Masquelier and Thorpe, 2007) and in the adult function of many circuits, including in humans (Testa-Silva, 2010; Arai et al., 2011; Casula et al., 2016). Pairing sensory stimulation with intracellular current injection has shown that STDP can adjust synaptic strength *in vivo* in different organisms and sensory systems (Froemke and Dan, 2002; Jacob et al., 2007; Dahmen et al., 2008; Hu et al., 2020). It is known that synaptic connectivity changes due to STDP are present in many systems, but whether STDP is a mechanism for adjusting sensory tuning remains controversial.

Despite the simplicity and known effectiveness of STDP as a mechanism for altering synaptic strength, the role of STDP in sensory processing or behavior is confounded by several additional factors that also affect synaptic plasticity. Synaptic firing rate, postsynaptic voltage, and synaptic cooperativity are known to affect the outcome of long-term plasticity (Lisman and Spruston, 2005, 2010; Feldman, 2012). Many studies of STDP are conducted *in vitro*, where the concentration of things like calcium in the media is altered and the reduced preparation does not reflect how the neuron would behave *in vivo* under natural conditions. To bridge the gap between STDP observed *in vitro* and its relevance to sensory processing and behavior *in vivo* would require replicating behaviorally relevant temporal patterns of synaptic activity *in vitro* and inducing the same patterns during sensory stimulation *in vivo*. However, the complex relationship between

sensory stimuli and the resulting patterns of synaptic input to central sensory neurons makes this challenging in many sensory systems. Using mormyrid weakly electric fish, I addressed how STDP affects sensory processing and behavior by studying a sensory pathway in which I could precisely control the timing of synaptic input *in viv*o, using the same stimulation patterns as previous *in vitro* experiments.

1.3 Temporal Coding of Electric Communication Signals in Mormyrid Fish

Mormyrid weakly electric fish produce and receive electric organ discharges (EODs) that they use to electrolocate and communicate. EODs have two salient features: waveform, which signals sender identity, and inter-pulse interval (IPI), which signals contextual information (Carlson, 2002). Mormyrids have a sensory pathway dedicated to processing electric communication signals (Xu-Friedman and Hopkins, 1999; Baker et al., 2013). The waveform of each EOD is encoded into spike timing differences among peripheral electroreceptors called knollenorgans (KOs), while interspike intervals within KOs encode IPIs (Baker et al., 2013). The KO afferent fibers project to the nucleus of the electrosensory lateral line lobe (nELL) in the hindbrain, where corollary discharge inhibition blocks responses to the fish's own EOD but not to external EODs generated by other fish (Bell and Grant, 1989). The nELL projects to the anterior exterolateral nucleus (ELa), a nucleus within a structure called the Torus Semicircularis (TS) (Amagai, 1998; Amagai et al., 1998; Baker et al., 2013). The TS is homologous to the mammalian inferior colliculus. The ELa has two cells types, inhibitory large cells and excitatory small cells, which both receive excitatory nELL input. EOD waveform tuning originates in the ELa small cells (Xu-Friedman and Hopkins, 1999; Lyons-Warren et al., 2013a). ELa small cells provide topographic, excitatory input to multipolar cells in the posterior exterolateral nucleus (ELp)

(Amagai, 1998; Amagai et al., 1998), another nucleus within the TS. Single neuron tuning to IPI arises in the ELp multipolar cells. Because ELa output precisely follows the timing of electric stimulus pulses (Hopkins and Bass, 1981; Lyons-Warren et al., 2013a), it is possible to stimulate ELp *in vitro* and *in vivo* using the same temporal patterns. This allows us to have precise control of the timing of presynaptic input using behaviorally relevant stimuli *in vivo* and to replicate those temporal patterns *in vitro*.

Indeed, ELp multipolar cells show the same IPI tuning in response to direct ELa stimulation *in vivo* as they do to sensory stimulation (Carlson, 2009). Within the ELp, excitatory and inhibitory multipolar neurons shape tuning to EOD waveform and IPI (Baker et al., 2013). Excitatory multipolar cells form extensive inter-connections with each other (Ma et al., 2013). They are more likely to share an excitatory connection with cells having similar IPI tuning, and connections between cells with similar IPI tuning are stronger than connections between cells with dissimilar tuning (Ma et al., 2013). In addition, local excitatory connections between ELp multipolar cells are more common at short distances (Ma et al., 2013). The dense interconnections among these timing-sensitive cells and the temporal precision of afferent input to ELp motivated experiments to test whether STDP affects the topology of this network. In this thesis, I show that STDP can alter the synaptic responses of ELp neurons *in vivo*, but these changes did not reliably predict changes in sensory tuning. Analysis of variation in synaptic responses suggests that differences in local connectivity *in vivo*, relative to what has been previously observed *in vitro*, affect the direction of synaptic changes induced by STDP.

1.4 STDP in the midbrain electrosensory circuit *in vitro*

Previous work done in the Carlson lab explored STDP in the ELp *in vitro* (Ma and Carlson, unpublished). Using an *in vitro* whole-brain preparation (Fig 1.1 A), they tested for STDP by pairing extracellular focal stimulation of ELa with intracellular current injection into ELp multipolar cells. Focal presynaptic stimulation was paired with postsynaptic spiking at a range of delays from -80 to +80 ms pre-post (Fig 1.2 C). There was a clear change in the postsynaptic potential amplitude for delays in the range of -25 to +25 ms between the relative timing of EPSP peaks and postsynaptic action potential peaks. They found that there was an increase in the synaptic strength as the pre-leads-post delay approached zero and a decrease in the synaptic strength as the post-leads-pre delay approached zero, a Hebbian STDP pattern (Fig 1.1 C) (Markram et al., 1997; Bi and Poo, 1998). When focal presynaptic stimulation preceded postsynaptic stimulation by 20 ms repeatedly, excitatory postsynaptic potentials (EPSPs) were potentiated (Fig 1.1 B, D). When focal presynaptic stimulation followed postsynaptic stimulation by 10 ms repeatedly, EPSPs were depressed (Fig 1.1 B, D). There was no significant change in EPSP amplitude in three controls: no stimulation, presynaptic stimulation only, or postsynaptic stimulation only (Fig 1.1 D).

Experiments were also done using an array of stimulus electrodes for presynaptic stimulation rather than a single, focal glass stimulus electrode. The array consisted of four channels of bipolar stimulation (8 electrodes total). They placed this array in ELa, just anterior to the ELp border. The rest of the stimulus protocol described above for the focal glass stimulus electrode was the same for the array stimulus electrodes. Using array presynaptic stimulation (Fig 1.2A), the resulting changes in EPSP amplitude were more variable than predicted based on results from focal presynaptic stimulation. No large changes in EPSP amplitude were observed for relatively long pre-leads postsynaptic delays or long post- leads presynaptic delays. However, at relatively short

pre-leads-post delays, both potentiation and depression were observed, and a similar pattern was observed at relatively short post-leads-pre delays (Fig 1.2B). These results show that stimulating a larger, more diffuse population of ELa neurons can result in a more variable pattern of STDP at both positive and negative pre-post delays close to zero, as compared to focal ELa stimulation. Comparing the normalized change in EPSP amplitude, they found that the -20 ms pre-post synaptic pairing was not significantly different from the +10 ms pre-post synaptic pairing (Fig 1.2C). After showing that STDP can alter synaptic connectivity *in vitro*, this motivated me to explore whether STDP alters sensory network connectivity *in vivo*.

Using the electrosensory system, I was able to connect STDP-induced changes in synaptic physiology and plasticity in sensory systems. I determined that STDP does alter synaptic connectivity *in vivo*. Although there was previous data showing that STDP altered synaptic connectivity and inter-pulse interval tuning *in vitro*, I found that disparities in the presence of clear Hebbian STDP *in vivo* is likely associated with differences in synaptic potential shape, which reflects differences in inhibition and polysynaptic activity. Altogether, I have shown that a common mechanism studied *in vitro* for how synaptic and network connectivity is altered does not always clearly map to how the same mechanism affects sensory tuning *in vivo*.

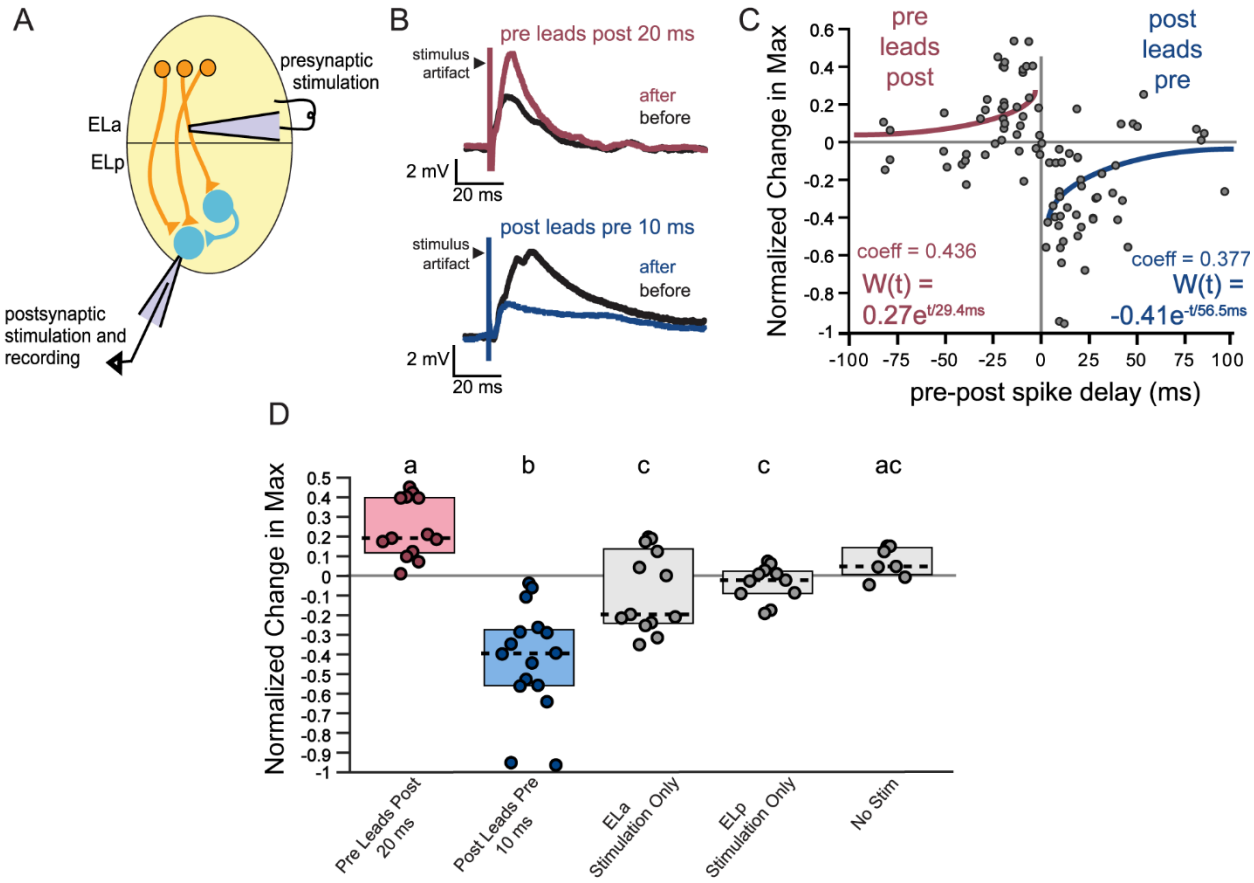

Figure 1.1. STDP alters synaptic connectivity in vitro. (A) Schematic of the *in vitro* set up showing focal microstimulation of ELa along with intracellular recording and current injection in ELp. (B) Example raw data traces collected in B. niger before and after pairing of a -20 ms pre-post delay in red and a +10 ms pre-post delay in blue. (C) Scatter plot of percent change in excitatory postsynaptic potential (EPSP) amplitude in ELp after pairing ELa stimulation with intracellular current-induced spiking in ELp neurons in *B. niger*. X-axis is the relative timing of EPSP peaks and postsynaptic action potential peaks. Exponential curve fits with equations are provided. (D) Normalized change in EPSP amplitude with median (black dotted line) & quartiles (boxes) for -20 ms pre-post delay in red (n = 12), +10 ms pre-post delay in blue (n=16), and all three controls in grey (ELa only n = 13, Intracellular only n = 11, No stimulus n = 7). Letters represent statistically significant differences between groups ($p<0.05$, one-way ANOVA followed by Tukey's HSD post-hoc test).

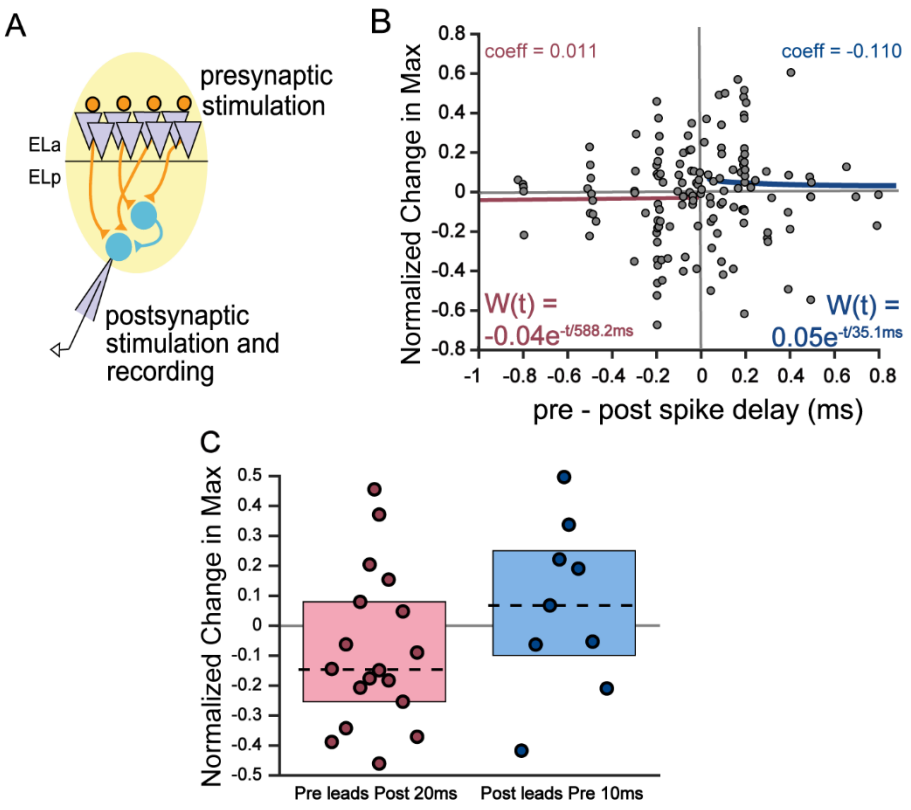

Figure 1.2. Stimulating ELa using an array electrode reveals more variation in STDP compared to focal stimulation *in vitro* (A) A schematic of the *in vitro* array set up showing 4-channel stimulation of ELa along with intracellular current injection in ELp. (B) Scatter plot of normalized change in EPSP amplitude in ELp after ELa array stimulation, data collected in *B. niger*. X-axis is the relative timing of EPSP peaks and postsynaptic action potential peaks. (n = 128). (C) Normalized change in EPSP max after pairing ELa array stimulation with intracellular current-induced spiking in ELp neurons at a -20 ms pre-post delay (left) and a +10 ms pre-post delay (right), showing the median (black dotted line) & quartiles (boxes) under control conditions (red, n = 18; blue, n = 9).

CHAPTER 2

Spike-timing-dependent plasticity alters electrosensory neuron synaptic strength *in vivo*

Authors:

Adalee Lube and Bruce Carlson

Author affiliations:

Department of Biology, Washington University in Saint Louis, MO, 63130, USA

2.1 Abstract

I addressed the role of spike-timing-dependent plasticity in driving changes in synaptic strength in a sensory pathway *in vivo*. It is challenging to precisely control temporal patterns of synaptic activity *in vivo* and replicate those patterns *in vitro*. This makes it difficult to make connections between STDP-induced changes in synaptic physiology *in vitro* and *in vivo*. Mormyrid weakly electric fish produce and receive electric organ discharges (EODs) that they use for electrolocation and communication. Because midbrain electrosensory neuron output precisely follows the timing of electric stimulus pulses received by the electrosensory peripheral sensory receptors, I could control the timing of synaptic input *in vivo* to replicate temporal patterns of synaptic input that were shown to induce STDP *in vitro*. Using whole-cell intracellular recordings in awake, behaving fish, I paired sensory stimulation with postsynaptic spiking using delays that reliably induced potentiation or depression *in vitro*. I found that STDP does alter synaptic strength *in vivo*, however, the change in synaptic responses induced by sensory stimulation *in vivo* did not always adhere to the direction predicted by the STDP previously observed *in vitro*. Further analysis suggests that this difference is influenced by polysynaptic activity, including inhibitory interneurons. STDP does alter synaptic responses to sensory stimulation *in vivo* but how the relationship of how STDP alters synaptic responses *in vivo* compared to previous work *in vitro* is complex.

2.2 Introduction

Spike-timing-dependent plasticity (STDP), in which synapse strength changes based on the relative timing of pre- and post-synaptic spiking, has been implicated in changes in neuronal connectivity hypothesized to underlie learning and memory (Markram et al., 1997; Song et al., 2000; Bi and Poo, 2001; Feldman, 2012). Despite intense interest in the role of STDP in many processes, STDP is rarely directly studied *in vivo* as a mechanism to modify neuronal sensory responses in adult organisms in real time. This is challenging to do because it requires bridging experiments *in vitro* and *in vivo* by using the same temporal patterns of synaptic activity in both. While this hurdle eliminates nearly all model systems, mormyrid weakly electric fish circumvent this issue. Mormyrids produce and receive electric organ discharges that they use to electrolocate and communicate. Peripheral electroreceptors respond with a single spike in response to each EOD and relay these precisely timed spikes to central sensory neurons (Hopkins and Bass, 1981; Lyons-Warren et al., 2012; Baker et al., 2013). Thus, there is a 1:1 relationship between stimulus (EOD) and synaptic input to these neurons.

Multipolar cells in the posterior exterolateral nucleus (ELp) exhibit the same inter-pulse interval (IPI) tuning to sensory stimulation as they do to direct electrical stimulation of the anterior exterolateral nucleus (ELa) (Carlson, 2009), the ELp's presynaptic input. This allows for stimulation in the ELp *in vivo* and *in vitro* with the exact same temporal patterns (Carlson, 2009; George et al., 2011; Ma et al., 2013; Baker and Carlson, 2014; Kohashi and Carlson, 2014). As with classic studies of Hebbian STDP (Markram et al., 1997; Bi and Poo, 1998; Song et al., 2000), the Carlson lab recently showed, using a whole-brain *in vitro* preparation, that presynaptic spikes in the ELa repeatedly leading postsynaptic spikes in the ELp leads to synaptic potentiation, whereas depression results when this sequence is reversed (Ma and Carlson, unpublished; Fig.

1.1). Because of the advantages of the mormyrid electrosensory system that allow for *in vivo* and *in vitro* stimulation with the same temporal patterns, I wanted to test if responses in the ELp could be shifted via STDP in a similar way *in vitro* and *in vivo*. Using intracellular, whole cell recordings, I paired presynaptic (sensory) stimuli with postsynaptic spiking at both pre-leads postsynaptic and post-leads presynaptic delays. I found that STDP altered sensory responses *in vivo*, but that differences in the results compared to the hypothesis created from the *in vitro* experiments are possibly due to more inhibition and polysynaptic activity seen *in vivo* compared *in vitro*. These experiments will contribute to our understanding of how STDP induces changes in synaptic strength that alter responses to natural sensory stimuli.

2.3 Results

2.3.1 STDP altered synaptic connectivity *in vivo*

I sought to determine whether STDP could be induced *in vivo* in response to pairing sensory stimuli with postsynaptic spiking. In these experiments in *Brevimyrus niger*, I provided presynaptic input using sensory stimulation while recording intracellularly from ELp neurons (Fig. 2.1A). I paired sensory stimulation with intracellular stimulation using delays that generally resulted in strong potentiation (-20 ms pre-post) vs. depression *in vitro* (+10 ms pre-post). However, for both pairings, I added a 3 ms delay to account for the latency between sensory stimulation and ELa responses (Amagai et al., 1998). Thus, I delivered paired stimulation with sensory stimulation leading postsynaptic stimulation by 23 ms, and sensory stimulation following postsynaptic stimulation by 7 ms, as well as three controls: sensory stimulation only, intracellular stimulation only, and no stimulation.

While many of the changes in synaptic responses fit the predicted patterns of potentiation in response to the sensory-leads-post pairing and depression in response to the post-leads-sensory pairing, many others did not (Fig. 2.1B). To quantify the change in the sensory responses after pairing, I measured the max of the postsynaptic potential (PSP) in a window from the end of the stimulus to 200 ms. In this same window, I measured the PSP area over time by summing the post-stimulus synaptic potential trace and multiplied by one over the sampling frequency (1/sampling frequency = sampling period). The change in the max and area calculations were normalized by subtracting the before pairing value from the after pairing value, then dividing by the maximum of the absolute values of the after pairing and before pairing values.

No significant differences were found among the 5 treatments for normalized change in PSP maximum values (Fig. 2.1C; $p = 0.089$, one-way ANOVA). However, there were significant differences among the treatments for normalized change in area (Fig. 2.1D; $p = 0.002$, one-way ANOVA). In particular, the sensory-leads-post pairing was significantly larger than the post-leads-sensory pairing (Fig. 2.1D; $p = 0.009$, Tukey's HSD). Results of the other pairwise comparisons are as follows: sensory-leads-post v. sensory stimulus only, $p = 0.466$; sensory-leads-post v. intracellular only, $p = 0.002$; sensory-leads-post v. no stimulus, $p = 0.088$; post-leads-sensory v. sensory stimulus only, $p = 0.404$; post-leads-sensory v. intracellular only, $p = 0.998$; post-leads-sensory v. no stimulus, $p = 0.934$; sensory only v. intracellular only, $p = 0.222$; sensory only v. no stimulus, $p = 0.880$; intracellular only v. no stimulus, $p = 0.807$ (all pairwise comparisons using Tukey's HSD).

To analyze the time course of these changes in synaptic responses, I subtracted the mean voltage trace before pairing from the mean voltage trace after pairing, and then averaged across neurons to obtain a mean difference potential that represents the overall time course of changes in

synaptic response. The maximum change in synaptic response occurred at 14.5 ms following stimulus onset for sensory-leads-post and 13.4 ms for post-leads-sensory (Fig 2.2A). Although there is a positive peak in the post-leads-sensory trace, the positive peak in the sensory-leads-post trace is larger, which shows there is a relative increase in synaptic strength in the sensory-leads-post delay relative to the post-leads-sensory delay. In addition, due to the later shape of the post-leads-sensory delay PSP, which reveals a decrease in synaptic strength, the overall change in area is closer to zero for the post-leads-sensory trace. I also analyzed the normalized change in onset slope and found no significant differences (Fig. 2.2B; $t(61) = 1.36$, $p = 0.178$, unpaired t-test).

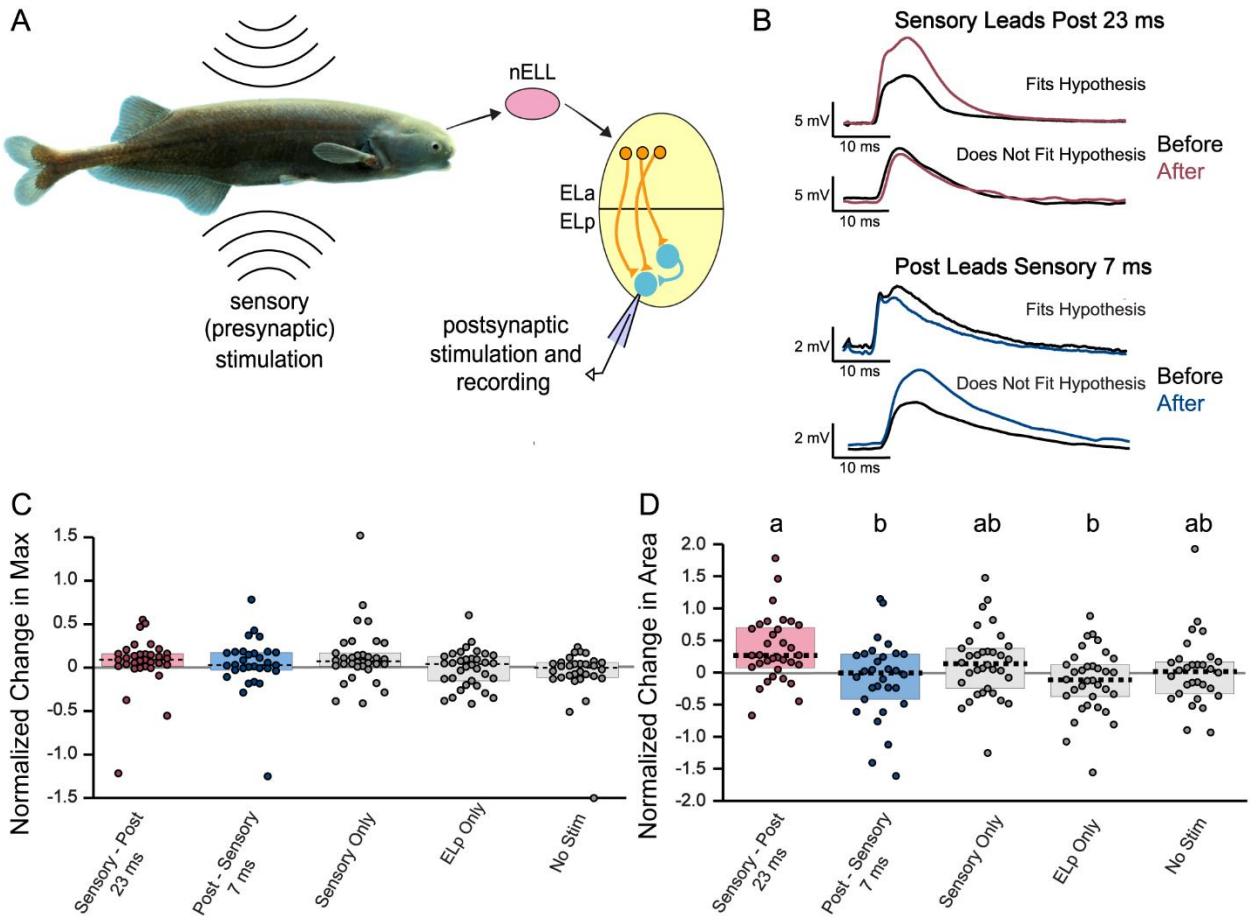

Figure 2.1. STDP alters synaptic connectivity *in vivo*. (A) A model of the *in vivo* set up showing sensory stimulation along with intracellular current injection in ELp. (B) Example raw data traces collected in *B. niger*, before and after pairing of a -23 ms sensory-post delay in red and a +7 ms sensory-post delay in blue. One example each of changes that fit the STDP pattern observed *in vitro* and that do not fit the STDP pattern observed *in vitro* are shown. (C) Normalized change in max (after-before) values with median (black dotted line) & quartiles (boxes) for -20 ms sensory-post delay in red (n = 33), 10 ms sensory-post delay in blue(n=30), and all three controls in grey (Sensory only n = 34, Intracellular only n = 34, No stimulus n = 30). (D) Same as in (C) but showing normalized change in area values rather than normalized change in max values. Letters represent statistically significant differences between groups ($p<0.05$, one-way ANOVA followed by Tukey's HSD post-hoc test).

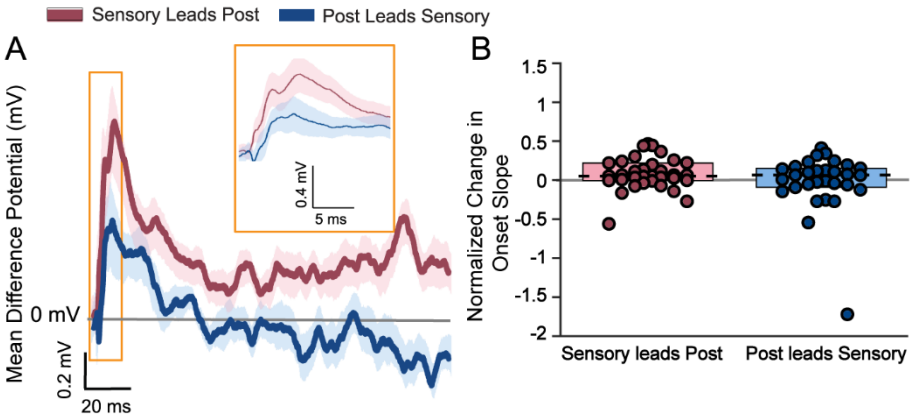

Figure 2.2. STDP affects synaptic activity later than 7 ms after stimulus onset. (A) Average After pairing – Before pairing traces collected in B. niger for – 23 ms sensory-post delay (red) and +7 ms sensory-post delay (blue). Time = 0 at stimulus onset. Grey line is zero mV. Lighter colored area surrounding the traces represent SEM. Inset is a zoomed in view of the area surrounding the peaks of the traces. (B) Normalized change in onset slope for *in vivo* data (-23 ms sensory-post delay in red (n = 33), +7 ms sensory-post delay in blue (n=30))

2.3.2 The induction of STDP varied with the physiological characteristics of synaptic responses

While the postsynaptic potentials recorded *in vitro* typically consisted almost exclusively of excitatory postsynaptic potentials with a single peak, the postsynaptic potentials recorded *in vivo* often contained both positive and negative components consisting of multiple peaks and troughs (Fig. 2.3). To determine whether there are physiological attributes of neurons that might relate to the widespread variation I observed in STDP during *in vivo* sensory stimulation (see Figs. 2.1B-D), I measured 32 landmarks from the postsynaptic potentials of each neuron before pairing (see the Experimental Procedures for details and a numbered list for reference; Fig. 2.5). I performed a Principal Components Analysis (PCA) on these landmarks and then ran a two-way ANOVA on the resulting PC scores in which the independent variables included pairing (pre-leads-post vs. post-leads-pre), and whether or not the observed change in postsynaptic potential after pairing fit our STDP predictions based on the normalized change in max data (i.e. a positive change in normalized max for a pre-leads-post delay and a negative change in normalized max for a post-leads-pre delay would fit our hypothesis; Fig 2.4). The specific eigenvalue loadings and the landmarks they represent can be found in Table 2.1.

There were N = 24 sensory-leads-post pairings that fit the hypothesis and N = 9 that did not fit. There were N = 13 post-leads-sensory pairings that fit the hypothesis and N = 17 that did not fit. The first four PC scores captured 76.31% of the variance. I found significant differences in PCs 2 and 3. There was a significant difference in PC2 between, the 'pairing' conditions (Fig. 2.4; $F(1,59) = 4.598$, $p = 0.036$, two-way ANOVA). There was a significant difference in PC3 between the 'fit' conditions (Fig. 2.4; $F(1,59) = 4.162$, $p = 0.046$, two-way ANOVA). Although the loadings did not separate into easily discernable categories (Table 2.1), there were significant differences

in the shapes of PSPs before pairing between neurons that fit our hypothesis and neurons that did not. Together, these results suggest that physiological characteristics of postsynaptic potential responses relate to whether the induction of STDP results in synaptic connectivity changes in the direction predicted by the *in vitro* focal stimulation results.

2.4 Discussion

In vitro studies across many brain regions and organisms reveal that repeated pre-leads postsynaptic spiking induces synaptic potentiation, whereas the reverse timing induces synaptic depression (Markram et al., 1997; Bi and Poo, 1998; Song et al., 2000). This Hebbian form of STDP has been implemented in a variety of computational models that explore many circuits (Song et al., 2000; Morrison et al., 2008; Huang and Wei, 2021). However, the role of STDP in the processing of behaviorally relevant stimuli in intact adult circuits remains controversial. I explored sensory processing in a system where I have precise control over the timing of presynaptic input using behaviorally relevant stimuli both *in vitro* and *in vivo*.

Recording intracellularly, I delivered sensory stimulation leading postsynaptic stimulation by 23 ms, and sensory stimulation following postsynaptic stimulation by 7 ms, as well as three controls: sensory stimulation only, intracellular stimulation only, and no stimulation. Unlike the focal *in vitro* data, no significant differences were found among the 5 treatments when measuring the change in normalized change in PSP maximum values (Fig. 2.1C). Unlike previous *in vitro* experiments though, the PSPs I observed *in vivo* did not exclusively consist of single, excitatory depolarizations. I observed a variety of potential shapes, often with multiple peaks and troughs (Fig 2.3). To attempt to holistically measure all changes due to STDP, I measured the PSP area in

addition to the maximum. There were significant differences among the treatments for normalized change in area (Fig. 2.1D).

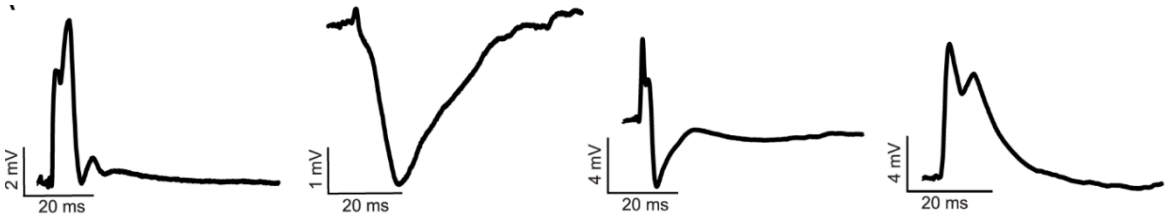

Figure 2.3. Variation in the effect of STDP is correlated with variation in synaptic responses. Raw trace examples of postsynaptic potentials recorded *in vivo* in *B. niger*.

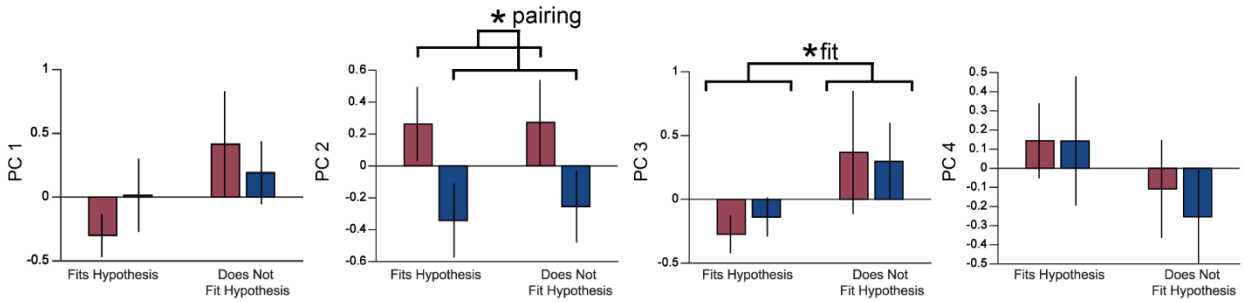

Figure 2.4 Principal components (PC) 1-4 for the *in vivo* data that 'fits' or 'does not fit' the STDP hypothesis based on the *in vitro* data for both -23 ms sensory-post delay (red) and +7 ms sensory-post delay (blue). Asterisks represent a significantly different variable or interaction stated in the text.

PC 1			PC 2			PC 3			PC 4		
4.	NumTroughs	6.91008	14.	RangeOffsetSlopeDep	4.86013	14.	MedianOnsetSlopeDep	2.85455	5.	MedianPeak	2.33251
2.	NumHyp	5.99544	5.	RangePeak	4.84126	14.	MedianOffsetSlopeDep	2.77874	14.	MedianOnsetSlopeHyp	2.10132
15.	SumTotalAreaHyp	5.95344	14.	RangeOnsetSlopeDep	4.76934	13.	MedianWHMinHyp	2.7589	10.	RangeDurHyp	1.83702
8.	RangelatenciesPT	5.5785	9.	RangeDurationDep	4.51542	10.	MedianDurHyp	2.51958	13.	RangeWHMinHyp	1.82815
11.	TotalPSPDur	5.55927	1.	NumDep	4.4765	5.	MedianPeak	2.44167	6.	MedianTrough	1.81151
16.	TotalArea	5.53596	3.	NumPeaks	4.29371	15.	SumTotalAreaDep	1.81764	14.	MedianOnsetSlopeDep	1.80741
10.	RangeDurHyp	5.24209	7.	RangeLatsDepsHyps	3.15481	9.	MedianDurationDep	1.81332	9.	MedianDurationDep	1.61062
13.	RangeWHMinHyp	5.23101	8.	MedianlatenciesPT	2.9138	11.	TotalPSPDur	1.57084	14.	RangeOffsetSlopeHyp	1.55087
6.	RangeTrough	4.86539	8.	RangelatenciesPT	2.90935	16.	TotalArea	1.26289	7.	RangeLatsDepsHyps	1.51278
7.	RangeLatsDepsHyps	4.48799	12.	RangeWHMaxDep	2.73333	14.	MedianOffsetSlopeHyp	1.20232	7.	MedianLatsDepsHyps	1.4479
8.	MedianlatenciesPT	4.46609	15.	SumTotalAreaDep	2.73042	8.	RangelatenciesPT	0.96092	15.	SumTotalAreaDep	1.44388
14.	RangeOnsetSlopeHyp	4.03482	11.	TotalPSPDur	2.24395	8.	MedianlatenciesPT	0.64584	14.	MedianOffsetSlopeDep	1.29975
7.	MedianLatsDepsHyps	3.43737	7.	MedianLatsDepsHyps	2.17771	5.	RangePeak	0.53852	2.	NumHyp	1.14989
14.	RangeOffsetSlopeHyp	2.91145	12.	MedianWHMaxDep	2.16824	14.	RangeOnsetSlopeDep	0.49817	12.	MedianWHMaxDep	0.8745
10.	MedianDurHyp	1.96495	14.	MedianOnsetSlopeHyp	1.22248	15.	SumTotalAreaHyp	0.48439	14.	NumTroughs	0.22232
14.	MedianOffsetSlopeHyp	1.44754	13.	MedianWHMinHyp	0.86689	14.	RangeOffsetSlopeDep	0.4426	14.	RangeOnsetSlopeHyp	0.08074
13.	MedianWHMinHyp	1.27482	2.	NumHyp	0.75164	14.	RangeOffsetSlopeHyp	0.21551	8.	MedianlatenciesPT	0.06914
14.	MedianOffsetSlopeDep	0.41972	10.	MedianDurHyp	0.5398	3.	NumPeaks	0.1554	14.	MedianOffsetSlopeHyp	0.06709
12.	RangeWHMaxDep	-0.1609	6.	MedianTrough	0.43279	1.	NumDep	-0.1824	3.	NumPeaks	0.03886
5.	MedianPeak	-0.2997	10.	RangeDurHyp	0.42794	13.	RangeWHMinHyp	-0.298	1.	NumDep	-0.0403
14.	MedianOnsetSlopeDep	-0.3833	13.	RangeWHMinHyp	0.3962	14.	MedianOnsetSlopeHyp	-0.316	12.	RangeWHMaxDep	-0.0633
12.	MedianWHMaxDep	-0.9507	9.	MedianDurationDep	0.38573	10.	RangeDurHyp	-0.352	8.	RangelatenciesPT	-0.1182
9.	RangeDurationDep	-1.1498	14.	RangeOnsetSlopeHyp	0.26125	12.	MedianWHMaxDep	-0.3754	5.	RangePeak	-0.401
9.	MedianDurationDep	-1.1803	4.	NumTroughs	0.12204	9.	RangeDurationDep	-0.405	9.	RangeDurationDep	-0.5402
14.	RangeOffsetSlopeDep	-1.513	14.	RangeOffsetSlopeHyp	0.04996	2.	NumHyp	-0.5484	14.	RangeOffsetSlopeDep	-0.5734
5.	RangePeak	-1.5225	14.	MedianOffsetSlopeHyp	-0.0652	6.	MedianTrough	-0.6696	11.	TotalPSPDur	-0.5965
14.	RangeOnsetSlopeDep	-1.6251	16.	TotalArea	-0.3001	4.	NumTroughs	-0.683	14.	RangeOnsetSlopeDep	-0.5987
14.	MedianOnsetSlopeHyp	-1.8124	6.	RangeTrough	-0.4107	7.	RangeLatsDepsHyps	-0.7367	16.	TotalArea	-0.9552
15.	SumTotalAreaDep	-2.4262	5.	MedianPeak	-1.1344	12.	RangeWHMaxDep	-0.9895	6.	RangeTrough	-1.1024
3.	NumPeaks	-2.6615	15.	SumTotalAreaHyp	-1.2804	7.	MedianLatsDepsHyps	-1.0315	15.	SumTotalAreaHyp	-1.405
1.	NumDep	-2.8658	14.	MedianOnsetSlopeDep	-1.6531	14.	RangeOnsetSlopeHyp	-1.5044	13.	MedianWHMinHyp	-2.0772
6.	MedianTrough	-3.5132	14.	MedianOffsetSlopeDep	-1.7844	6.	RangeTrough	-1.6158	10.	MedianDurHyp	-2.4615

Table 2.1 Synaptic potential landmarks and their respective eigenvalue loadings for PCs 1-4, referenced in Fig. 2.4. For each PC, the loadings are ordered from largest to smallest.

When analyzing the time course of postsynaptic potential changes, I showed that the peak of synaptic potential change for both sensory-leads-postsynaptic delays and postsynaptic–leads-sensory delays occurs more than 10 ms after stimulus onset (Fig. 2.2A). Previous work has shown that ELa response latencies to sensory stimuli are 2.5 - 3 ms (Amagai et al., 1998), and ELp response latencies to sensory stimuli are 7 to 20 ms (Amagai, 1998). Thus, the changes in synaptic potential *in vivo* occur in a timeframe consistent with changes at ELp-to-ELp synapses.

I also measured the onset slope of PSPs (Fig. 2.2B). Previous work has shown that the onset slope of a PSP represents the immediate upstream pre-synaptic glutamate synapse (Taube and Schwartzkroin, 1988), which in this case would be direct synapses from the ELa. I found no significant changes in onset slope following STDP, consistent with STDP acting at ELp-to-ELp synapses rather than ELa-to-ELp synapses. STDP acting at these synapses may also explain why ELp neurons with similar IPI tuning are more likely to share an excitatory synaptic connection, and why these excitatory synapses are stronger, compared to neurons with dissimilar IPI tuning (Ma et al., 2013).

Recently, Chindemi et al. (Chindemi et al., 2022) showed that modeling LTP/LTD in pyramidal cells in the neocortex based on *in vitro* stimulation protocols created stereotypical potentiation and depression as expected, but when the model was adjusted for physiological levels of calcium, LTP/LTD magnitudes were greatly reduced and required higher frequency stimulation to achieve. Further experiments manipulating the calcium concentration or stimulation frequency *in vivo* could be done to further elucidate what could be contributing to the discrepancy between our *in vivo* results and *in vitro* focal stimulation results. Alternative types of plasticity could also be involved. For example, the presence of synaptic clustering through cooperative plasticity allows for local plasticity in a group of functionally similar neurons (Mehta, 2004; Harvey and Svoboda,

2007; Larkum and Nevian, 2008). A well-studied mechanism in the field of memory formation (Kastellakis and Poirazi, 2019), the consequence of this cooperative plasticity would be an anatomically restrained plasticity, where only synapses close enough together on the postsynaptic dendrite would be potentiated by repeated activation (Mehta, 2004). Considering the dense interconnections and distinct tuning properties of ELp multipolar cells (Ma et al., 2013), it is possible that distinct clusters of synapses with different tuning properties and a differing presence of inhibition would all be affected by repeated stimulation variably.

In our system, previous work in the ELa has shown that a given EOD stimulates a unique population of ELa neurons (Baker et al., 2013; Lyons-Warren et al., 2013a), and that ELa provides topographic, excitatory input to ELp (Friedman and Hopkins, 1998). In addition, local excitatory connections between ELp multipolar cells are more common at short distances (Ma et al., 2013). Thus, focal ELa stimulation *in vitro* would drive activity in primarily local excitatory synapses between ELp neurons, in the topographic location corresponding to the ELa stimulation. Array stimulation *in vitro* and sensory stimulation *in vivo*, however, would stimulate a more diffuse population of ELa projection neurons, driving postsynaptic activity in multipolar cells across the ELp, including more inhibitory pathways leading to the recorded neuron than expected from focal ELa stimulation. A stereotypically potentiating delay of pre-leads postsynaptic activity could lead to visible depression in the postsynaptic response if the balance between excitatory and inhibitory pathways to the neuron was shifted towards inhibitory pathways. If these inhibitory pathways were more numerous or more affected by STDP, this would result in STDP in the opposite of the predicted direction.

To begin to address this hypothesis, I performed a landmark calculation and PCA analysis to determine whether physiological characteristics of synaptic responses correlated with variation

in the direction of synaptic potential change induced by STDP. I found that there were significant differences in the PC scores depending on the 'fit' of the data, i.e. whether or not the data followed the predicted direction of STDP (Fig 2.4). Importantly, the PC scores reflected landmarks related to the properties of depolarizations and hyperpolarizations present in an individual PSP, so differences in PC scores are suggestive of differences in the balance of excitatory and inhibition in data that 'fit' compared that data that do not. Thus, a significant difference in the PC scores suggests that more inhibition and polysynaptic activity could lead to a more diverse STDP response with sensory stimulation *in vivo* as compared to focal stimulation *in vitro*, as both excitatory and inhibitory synapses could be under the influence of STDP. In conclusion, though I did successfully induce statistically significant synaptic change *in vivo* in the direction predicted by Hebbian STDP, the variability I observed in the synaptic responses *in vivo* suggests that STDP rules at synapses *in vitro* do not always predict outcomes *in vivo*.

2.5 Experimental Procedures

2.5.1 Animals

In this study, I used a total of 37 *Brevimyrus niger* of both sexes, ranging from 4.5–9.4 cm in standard length. The Carlson lab acquired the fish through the aquarium trade and housed them in same-species groups with a 12:12 h light/dark cycle, water conductivity of 200–400 μS/cm, and a temperature of 25–29°C. The fish were fed live black worms four times per week. All procedures were in accordance with the guidelines established by the National Institutes of Health and were approved by the Institutional Animal Care and Use Committee at Washington University in St. Louis.

2.5.2 *In vivo* whole cell recording

I prepared fish for *in vivo* recordings from ELp as described previously (Carlson, 2009; Lyons-Warren et al., 2013b). Fish were anesthetized in 300 mg/L tricaine methanesulfonate (MS-222) and paralyzed with an intramuscular injection of 100 µl of 0.1 mg/ml gallamine triethiodide (Flaxedil). The fish was then moved to a recording chamber, where it was submerged in freshwater, except for a small region of the surface of the head. I maintained general anesthesia for surgery by respirating the fish with an aerated solution of 100 mg/ml MS-222 through a pipette tip in the mouth. The surgery site was anesthetized with 0.4% lidocaine on the skin. I then removed the skin of the surgery site, affixed a post to the skull, and removed a rectangular piece of skull covering ELp. I placed the ground electrode on the nearby cerebellum. After surgery, I brought the fish out of anesthesia by switching to aerated freshwater respiration and monitored the fish's electric organ discharge command (EODC) output with a pair of electrodes placed next to the fish's tail (Carlson, 2002, 2009; Lyons-Warren et al., 2013b; Baker et al., 2016). The EOD output is silenced by flaxedil (the muscle paralytic), but I recorded the EODC as a fictive EOD. MS-222 anesthesia silences the EODC output, so the return of EODC output indicates that the fish has recovered from anesthesia (Lyons-Warren et al., 2013b). At the end of the recording session, the respiration of the fish was switched back to 100 mg/L MS-222 until no EODC output could be recorded, and then the fish was sacrificed by freezing.

I obtained intracellular, whole-cell patch recordings in current-clamp using previously published methods (Rose and Fortune, 1996; Carlson, 2009; Baker and Carlson, 2014). I used glass patch micropipettes with resistances of 20–40 MΩ. The pipette tip was filled with a solution (in mM) of 100 CH_3CO_2K, 2 KCl, 1 $MgCl_2$, 5 EGTA, 10 HEPES, 20 KOH, and 43 biocytin, and the pipette shank was filled with the same solution, except that biocytin was replaced with D-mannitol

(Carlson, 2009; Baker and Carlson, 2014). Initial seal resistances were >1 GΩ. Recordings were amplified 10x and low-pass filtered (cutoff frequency, 10 kHz) using an Axopatch 200B amplifier (Molecular Devices), digitized at a rate of 97.7 kHz (Model RX8 Digitizer, Tucker Davis Technologies), and saved using custom software written in Matlab. I delivered electrosensory stimulation using electrodes positioned around the perimeter of the recording chamber (Lyons-Warren et al., 2013b).

2.5.3 Data collection

After patching a cell, I stimulated with bipolar square pulses, adjusting the duration (0.1–1.5 ms), intensity (3–71 mV/cm), polarity (normal or reversed), and stimulus orientation (transverse or longitudinal to the fish) to elicit maximal sub-threshold, postsynaptic potential (PSP) amplitudes from each neuron. Next, I injected intracellular, depolarizing current, adjusting the duration (1 to 8 ms) and amplitude (0.1 to 0.9 nA) until a reliable spike was produced in each neuron. All subsequent sensory and intracellular stimuli delivered during a trial then used these parameters. I did not include in the repetition count any responses to stimulus repetitions in which stimuli occurred within 2–5 ms after an EODC response, since corollary discharge inhibition in the hindbrain blocks sensory responses within this window (Bell and Grant, 1989). I only used recordings in which the resting potential varied by 5.5 mV or less across all trials and was at least –40 mV throughout the experiment.

The sensory stimulus was repeated 30 times to get an averaged post-synaptic potential baseline response. The sensory stimulation was then paired with intracellular current injection at the delay of maximum potentiation observed *in vitro*, -20 ms pre-post delay, or the delay of maximum depression, +10 ms pre-post delay. Three ms were added to each delay time to account

for the latency from knollenorgan stimulation to ELa evoked potential for final delays of -23 ms pre-post and +7 ms pre-post. There were three controls: sensory stimulation only, intracellular stimulation only, or no stimulation. All pairings, sensory stimulation only and intracellular stimulation only control conditions were repeated at 1 Hz for 6 minutes. The no stimulation control lasted 6 minutes. The order in which they were repeated was decided pseudo-randomly, to maintain an equal number of times that each of the 2 pairings and 3 controls were collected first. After every pairing or control, sensory stimulation was repeated 30 times to obtain an averaged post-synaptic potential to compare to baseline. To measure the max of the PSP, I found the maximum point in a window from the end of the stimulus to 200 ms. In this same window, to measure the PSP area over time, I summed the post-stimulus synaptic potential trace and multiplied by one over the sampling frequency (1/sampling frequency = sampling period).

2.5.4 Synaptic Potential Landmarks

In our *in vivo* experiments, I often observed multiple phases of depolarizations and hyperpolarizations during a post-synaptic potential. I wanted to quantify the physiological characteristics of these synaptic responses to see whether differences in those characteristics correlated with differences in the observed STDP. Synaptic potential landmarks were calculated on the pre-pairing (i.e. baseline) postsynaptic potential trace. The raw trace was filtered with a 2 ms median filter, and the 1^{st} and 2^{nd} derivative were both filtered with a 5 ms zero-phase digital filter. Resting potential was calculated by averaging the 50 ms prestimulus period. The baseline postsynaptic potential traces were zeroed by subtracting the resting potential value from the whole trace. The threshold for a depolarization or a hyperpolarization was +/- 3 standard deviations from the baseline mean, respectively. We measured 32 different landmarks from each PSP based on 16

different types of measurements. An example of a PSP illustrating these landmarks can be found in Figure 2.5. The landmarks are numbered, and the same numbers are used in Tables 2.1 for reference. These measurements behind these landmarks were defined and measured as follows:

1. **Total # of depolarizations**: # of points that crossed threshold with a positive slope (i.e. point (i-1) < threshold< point (i))
2. **Total # of hyperpolarizations**: # of points that crossed threshold with a negative slope (i.e. point (i-1) > threshold>point (i))
3. **Total # of peaks**: # of local maxima above threshold within a given depolarization, can be >1. The timing of each peak was also recorded. We also set a selection criterion to determine what constitutes a local maximum. We took the first derivative of the trace and recorded all the locations of sign changes in the first derivative trace. To be considered a local maximum, the peak magnitude had to be greater than the maximum value of the post-stimulus trace minus the minimum value of the post-stimulus trace, divided by 20, from above the first point of a sign change in the first derivative on either side of the peak in question (Yoder, 2022).
4. **Total # of troughs**: # of local minima below threshold within a given hyperpolarization, can be >1. The timing of each trough was also recorded. We also set a selection criterion to determine what constitutes a local minimum. We took the first derivative of the trace and recorded all the locations of sign changes in the first derivative trace. To be considered a local minimum, the trough magnitude had to be less than the maximum value of the post-stimulus trace minus the minimum value of the post-stimulus trace, divided by 20, from below the first point of a sign change in the first derivative on either side of the trough in question (Yoder, 2022).

5. **Median and range of values of peaks:** We measured the median and range (largest peak minus smallest peak) of all the peak amplitudes.
6. **Median and range of values of troughs:** We measured the median and range (largest trough minus smallest trough) of all the trough amplitudes.
7. **Median and range of latencies to all depolarizations and hyperpolarizations**: The beginning of a depolarization was defined as the timing of the maximum in the second derivative between the end of the previous depolarization or hyperpolarization and the first peak in the depolarization. If there was no preceding hyperpolarization or depolarization, then the timing of stimulus offset was used instead. The depolarization latency was defined as the beginning of a depolarization minus the time of stimulus offset. The beginning of a hyperpolarization was defined as the timing of the minimum in the second derivative between the end of the previous depolarization or hyperpolarization and the first trough in the hyperpolarization. If there was no preceding hyperpolarization or depolarization, then the time of stimulus offset was used instead. The hyperpolarization latency was defined as the beginning of a hyperpolarization minus the time of stimulus offset. The median and range were calculated for all the depolarization and hyperpolarization latencies combined.
8. **Median and range of latencies to all peaks and troughs**: The peak latency was defined as the timing of the peak minus the timing of stimulus offset. The trough latency was defined as the timing of the trough minus the timing of stimulus offset. The median and range were calculated for all the peak and trough latencies combined.
9. **Median and range of total duration of each depolarization**: Peaks in the second derivative were defined the same as peaks in the PSP (see above), but on the 2nd derivative trace (Yoder, 2022). The end of a depolarization was defined as the timing of the first peak in the second

derivative after the offset threshold crossing used to define the depolarization. End latency was defined as the end of a depolarization minus the timing of stimulus offset. The total duration of the depolarization was defined as the depolarization end latency minus the depolarization latency. The median and range were calculated for all the depolarization durations.

10. **Median and range of total duration of each hyperpolarization**: Troughs in the second derivative were defined the same as troughs in the PSP (see above), but on the 2nd derivative trace (Yoder, 2022). The end of a hyperpolarization was the time of the first trough in the second derivative after the offset threshold crossing used to define the hyperpolarization. End latency was defined as the end of a hyperpolarization minus the timing of stimulus offset. The total duration of the hyperpolarization was defined as the hyperpolarization end latency minus the hyperpolarization latency. The median and range were calculated for all the hyperpolarization durations.
11. **Total PSP duration**: Total PSP duration was defined as the end latency of the last depolarization/hyperpolarization minus the first depolarization/hyperpolarization latency.
12. **Median and range of duration at half max value of each depolarization**: First, we found the value at half of the max, which is the largest peak of a depolarization plus the magnitude at the depolarization latency, divided by two. Then, we found the timings of half max before and after the largest peak. The duration at half max equaled the timing of half max after peak minus the timing of half max before peak.
13. **Median and range of duration at half min value of each hyperpolarization**: First, we found the value at half of the min, which is the largest trough of a hyperpolarization plus the magnitude at the hyperpolarization latency, divided by two. Then, we found the timings of half

min before and after the largest trough. The duration at half min equaled the timing of half min after trough minus the timing of half min before trough.

14. **Median and range of onset and offset average slope of depolarizations and hyperpolarizations**: The depolarization onset slope was calculated by taking the largest peak magnitude of a depolarization minus the depolarization start magnitude, divided by the difference of time between those two points. The hyperpolarization onset slope was calculated by taking the largest trough magnitude of a hyperpolarization minus the hyperpolarization start magnitude, divided by the difference in time between those two points. The depolarization offset slope was calculated by taking the largest peak magnitude of a depolarization minus the depolarization end magnitude, divided by the difference in time between those two points. The hyperpolarization offset slope was calculated by taking the largest trough magnitude of a hyperpolarization minus the hyperpolarization end magnitude, divided by the difference in time between those two points.
15. **Summed area of depolarizations and hyperpolarizations**: The depolarizations area was calculated by summing all values above threshold then multiplying by multiplied by one over the sampling frequency (1/sampling frequency = sampling period). The hyperpolarizations area was calculated by summing all values below threshold and then multiplying by multiplied by one over the sampling frequency (1/sampling frequency = sampling period)
16. **PSP total area**: The total area was calculated by summing the total depolarizations area (from above) and the hyperpolarizations area (from above).

2.5.5 Statistical Analyses

Unless otherwise stated, values are represented as median and 75%/25% quartiles. The max and area were measured as described above for both baseline PSPs and the PSPs measured following pairing. The Area, Max, and Slope calculations were normalized by subtracting the after minus before value and dividing by the absolute value of the maximum of the after and before, multiplied by 100. A t-test was used if there were 2 groups or 1-way ANOVA if there were more than 2 groups. Details of the synaptic landmark measurements are found in the section above entitled Synaptic potential landmarks. A principal components analysis was performed on the landmarks measured. The first four principal components were retained for each. Statistical analysis was done in SPSS and Matlab.

2.6 Acknowledgements

I thank Xiaofeng Ma for completing the *in vitro* experiments that led to this work. Funded by NSF IOS 1755071.

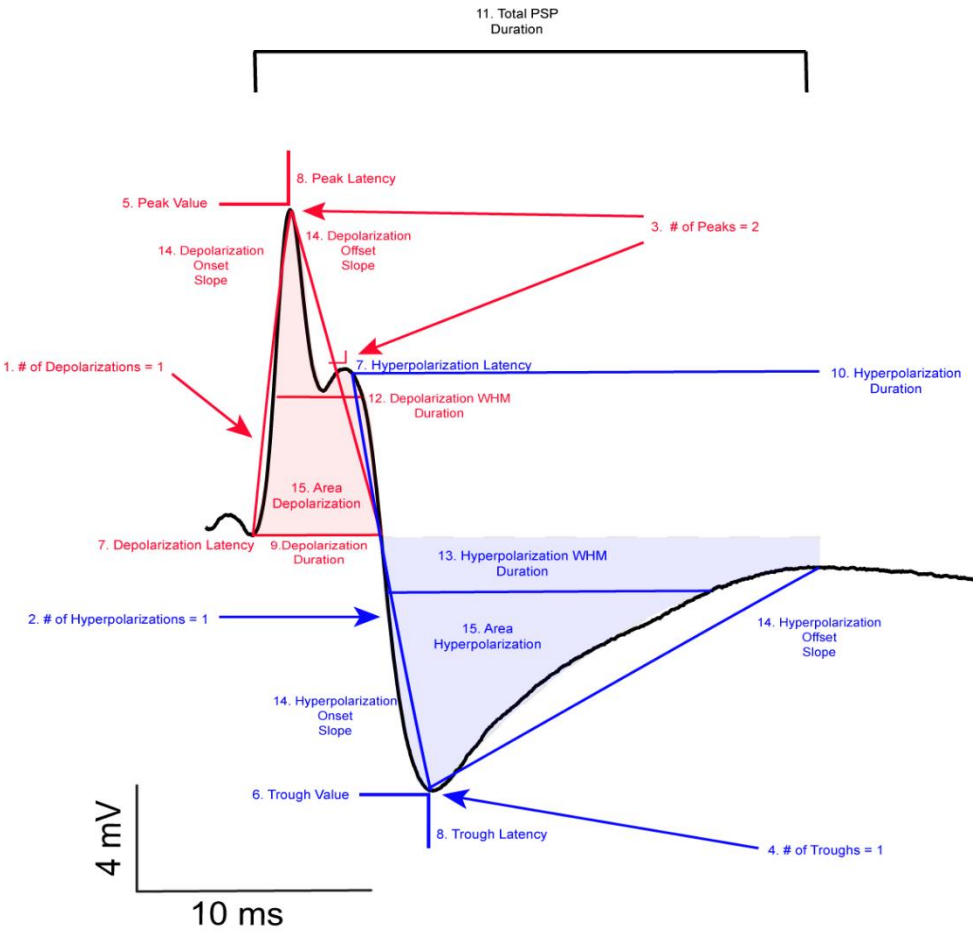

Figure 2.5 Synaptic potential landmarks labeled on an example postsynaptic potential *in vivo*.

CHAPTER 3

Spike-timing-dependent plasticity alters electrosensory neuron synaptic strength, but does not consistently alter sensory tuning *in vivo*

Authors:

Adalee Lube, Bruce A. Carlson

Author affiliations:

Department of Biology, Washington University in Saint Louis, MO, 63130, USA

3.1 Abstract

How do sensory systems optimize detection of behaviorally relevant stimuli when the sensory environment is constantly changing? I addressed the role of spike-timing-dependent plasticity (STDP) in altering sensory tuning. It is challenging to precisely control temporal patterns of synaptic activity *in vivo* and replicate those patterns *in vitro* in behaviorally relevant ways. This makes it difficult to make connections between STDP-induced changes in synaptic physiology and plasticity in sensory systems. Using mormyrid weakly electric fish, which produce electric organ discharges for electrolocation and communication, I could control the timing of synaptic input *in vivo* to replicate temporal patterns of synaptic input that were shown to induce STDP *in vitro*. Thus, I can manipulate sensory stimuli to precisely drive pre-synaptic spiking onto sensory neurons, allowing me to determine whether the induction of STDP is sufficient to shift neuronal tuning to changing sensory stimuli *in vivo*. Using whole-cell intracellular recordings in awake, behaving fish, I paired behaviorally relevant EOD and IPI patterns with a pre-leads postsynaptic spiking delay. I found that STDP did not alter sensory tuning *in vivo*, however, further analysis suggests that the difference in the sensory tuning results *in vivo* and *in vitro* is influenced by differing amounts of polysynaptic activity, including inhibitory interneurons, relative to previous *in vitro* work. Our findings suggest that STDP rules that alter inter-pulse interval tuning *in vitro* may not drive the same changes in sensory tuning *in vivo.*

3.2 Introduction

How does a sensory system optimize detection of behaviorally relevant stimuli amidst constant changes in those stimuli and to the sensory environment? To efficiently process sensory information, sensory systems are tuned to specific stimulus attributes. Rather than being tuned to every possible stimulus variant, a more efficient approach is for the neuronal tuning of a sensory system to adapt to changing stimulus statistics. Sensory systems are known to adapt to a variety of complex stimulus statistics, such as the probability of occurrence in the environment, stimulus rate, stimulus distribution, local stimulus mean, variation in stimulus statistics, intensity, and more (Wark et al., 2007; Sharpee et al., 2014). For example, retinal ganglion cells adjust their firing rate 2-5 fold in response to changes in image contrast, providing a mechanism for contrast adaptation (Smirnakis et al., 1997). In guinea pig auditory midbrain, the neuronal population as a whole shifts their responses to best encode commonly occurring sounds, though the mechanism for this shift remains unknown (Dean et al., 2005). Electrosensory pyramidal neurons in gymnotiform weakly electric fish respond maximally to low frequencies under local spatial stimulation, while they respond maximally to high frequencies under more global stimulation (Chacron et al., 2003). This may be due to different amounts of inhibitory input in these different stimulus contexts. A variety of examples exist showing shifts in neuronal tuning depending on behavioral context (Simoncelli and Olshausen, 2001; Wark et al., 2007; Solomon and Kohn, 2014; Whitmire and Stanley, 2016), but are there common mechanisms that could allow for tuning adaptation in a quickly changing sensory environment? Pairing sensory stimulation with intracellular current injection has shown that STDP adjusts synaptic strength *in vivo* in different organisms and sensory systems (Froemke and Dan, 2002; Jacob et al., 2007; Dahmen et al., 2008; Hu et al., 2020). It is known that synaptic

connectivity changes due to STDP are present in many systems, but whether STDP is a mechanism for altering sensory tuning in adult organisms in real-time remains controversial.

Mormyrid weakly electric fish produce and receive electric organ discharges (EODs) that they use to electrolocate and communicate. EODs have two salient features: waveform, which signals sender identity, and inter-pulse interval (IPI), which signals contextual information (Carlson, 2002). In the electric communication specific pathway, EOD waveform tuning originates in central sensory neurons in the anterior exterolateral nucleus (ELa) (Xu-Friedman and Hopkins, 1999; Lyons-Warren et al., 2013a). ELa provides topographic, excitatory input to the posterior exterolateral nucleus (ELp), where single-neuron IPI tuning is established (Carlson, 2009).

Within the ELp, excitatory and inhibitory multipolar neurons shape tuning to EOD waveform and IPI (Baker et al., 2013). Excitatory multipolar cells form extensive inter-connections with each other (Ma et al., 2013). They are more likely to share an excitatory connection with cells having similar IPI tuning, and connections between cells with similar IPI tuning are stronger than connections between cells with dissimilar tuning (Ma et al., 2013). In addition, local excitatory connections between ELp multipolar cells are more common at short distances (Ma et al., 2013).

Previous *in vitro* work in the lab tested whether STDP could elicit selective changes in the responses to different IPI stimuli (Ma and Carlson, unpublished; Fig. 3.1). They repeatedly delivered trains of 10 ms and 100 ms IPIs while pairing postsynaptic stimulation with just one of the IPIs at a pre-leads-post delay of -20 ms. They then measured the change in response to both 10 ms and 100 ms IPIs after pairing. They found clear evidence for a differential shift in responses to 10 vs. 100 ms IPIs depending on which IPI postsynaptic spikes were paired with, resulting in a significant ‘stimulus’ * ‘pairing’ interaction effect. Pairing with 10 ms IPIs led to a relative

increase in synaptic responses to 10 ms IPIs compared to 100 ms IPIs, whereas pairing with 100 ms IPIs led to a relative increase in synaptic responses to 100 ms IPIs compared to 10 ms IPIs (Fig 3.1).

Because ELa output precisely follows the timing of electric stimulus pulses (Hopkins and Bass, 1981; Lyons-Warren et al., 2013a), the ELp can be stimulated *in vitro* and *in vivo* with the exact same temporal patterns. Indeed, ELp multipolar cells show the same IPI tuning in response to direct ELa stimulation *in vitro* as they do to sensory stimulation (Carlson, 2009). It follows that tuning in the ELp could be shifted via STDP in a similar way *in vitro* and *in vivo*. Despite this, I show that STDP does not consistently alter sensory tuning *in vivo*. Analysis of variation in synaptic responses suggests that differences in local connectivity *in vivo* relative to *in vitro* affect the direction of synaptic changes induced by STDP.

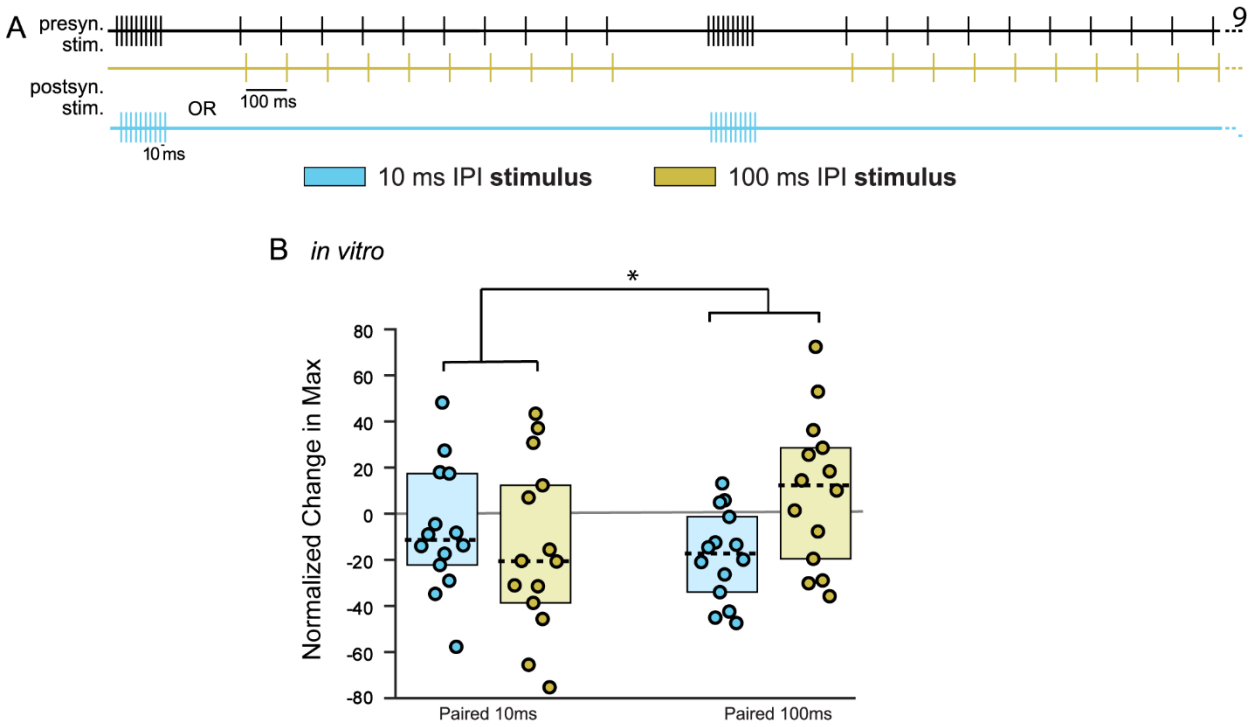

Figure 3.1. STDP alters IPI tuning *in vitro* (A) Model of the stimulation protocol, showing an alternating train of 10 ms and 100 ms IPIs in black with intracellular current injection in the ELp only paired with either the 10 ms IPI (blue, n = 14) or 100 ms IPI (yellow, n = 14). (B) *In vitro* normalized change in max amplitude values with median (black dotted line) & quartiles (boxes) for the paired IPI as compared to the unpaired IPI (N = 14 for all pairings. Data collected in *B. niger*. Asterisks represent statistically significant interaction effect between 'stimulus' * 'pairing' variables ($p<0.05$, two-way ANOVA). EPSP amplitudes were normalized by subtracting the before pairing values from the after pairing values, and then dividing by the maximum of the absolute values of the after pairing and before pairing values.

3.3 Results

3.3.1 STDP did not alter EOD tuning as predicted by *in vitro* focal stimulation data

I sought to determine whether STDP could elicit selective changes in the synaptic responses to particular EOD sensory stimuli. In this experiment in *Brienomyrus brachyistius*, I presented a randomly chosen conspecific EOD and a 90-degree phase-shifted version of that EOD as sensory stimuli. The latter manipulation maximally distorts the EOD waveform in the temporal domain while keeping the frequency spectrum constant (Hopkins and Bass, 1981; Carlson et al., 2011). After recording responses to both stimuli, I randomly selected one of the two stimuli to pair with intracellular stimulation at a -23 ms sensory-leads-post delay. I then recorded responses to both stimuli after pairing to determine whether there was a selective increase in synaptic response to the paired stimulus. To quantify the change in the sensory responses to EODs after pairing, I measured the max of the postsynaptic potential (PSP) in a window from the end of the stimulus to 200 ms. In the same window in which the max was calculated for the EOD, I measured the PSP area over time by summing the post-stimulus synaptic potential trace and multiplied by one over the sampling frequency (1/sampling frequency = sampling period). The change in the max and area calculations were normalized by subtracting the before pairing value from the after pairing value, then dividing by the maximum of the absolute values of the after pairing and before pairing values.

I found no significant differences for either the normalized change in area or the normalized change in max data (Fig. 3.2A and B). However, some experiments did result in selective increases in response to the paired stimulus, as seen by the grey lines connecting data points from the same neurons.

Within this sensory pathway, ELa neurons respond faithfully to a given EOD stimulus regardless of IPI, and IPI tuning first arises within ELp (Carlson, 2009). Thus, I was able to test whether STDP could elicit selective changes in the responses to different IPI stimuli. To quantify the change in the sensory responses to IPI trains after pairing, I measured the max of the PSP in a window from the end of the first stimulus in the IPI train to the start of the second stimulus in the IPI train. In the same window in which the max was calculated for the IPI, I measured the PSP area over time by summing the post-stimulus synaptic potential trace and multiplied by one over the sampling frequency (1/sampling frequency = sampling period). The change in the max and area calculations were normalized by subtracting the before pairing value from the after pairing value, then dividing by the maximum of the absolute values of the after pairing and before pairing values. In *Brevimyrus niger*, I repeatedly delivered trains of 10 ms and 100 ms IPIs while pairing postsynaptic stimulation with just one of the IPIs at or sensory-leads-post delay of -23 ms (Fig. 3.3A). I then measured the change in response to both 10 ms and 100 ms IPIs after pairing. There were no significant differences for changes in either the normalized max or area for the 10 ms or 100 ms IPI pairings (Fig. 3.3B and C).

3.3.2 Shifts in EOD and IPI tuning varied with the physiological characteristics of synaptic responses

Some EOD and IPI sensory tuning experiments did result in selective increases in response to the paired stimulus, as seen by the grey lines connecting data points from the same neurons (Figs. 3.2 and 3.3). Therefore, I performed a landmark calculation and PCA analysis on these data to determine whether physiological characteristics of synaptic responses could predict the shift in responses to paired and unpaired EOD and IPI stimuli. For the EOD tuning experiments, there

were N = 38 natural EOD pairings that fit the hypothesis and N = 32 that did not fit. There were N = 36 shifted EOD pairings that fit the hypothesis and N = 34 that did not fit. The first four PC scores captured 58.9% of the variance. PC1 and PC4 had significant 'fit'*'pairing' interactions (Fig. 3.4A; $F(1,136) = 7.03$, $p = 0.009$, two-way ANOVA and $F(1,136) = 6.59$, $p = 0.011$, two-way ANOVA). In the eigenvalue loadings found in Table 3.1, for PC1, negative loadings are dominated by landmarks relating to depolarizations, while positive loadings are dominated by landmarks relating to hyperpolarizations. This suggests that the relative balance of excitatory and inhibitory pathways leading to the recorded neuron is affecting whether the EOD tuning data fit the STDP direction predicted by the focal *in vitro* data.

For PC4, although the loadings did not separate into easily discernable categories, there were still significant differences in the PC, which suggests that differences in synaptic potential landmarks relate to whether the EOD tuning data did or did not fit the expected STDP direction based on the focal *in vitro* data.

For the IPI tuning experiments, there were N = 7 10 ms pairings that fit the hypothesis and N = 11 that did not fit. There were N = 7 100 ms pairings that fit the hypothesis and N = 10 that did not fit. The first four PC scores captured 71% of the variance. The specific eigenvalue loadings and the landmarks they represent can be found in Table 3.2. There were no significant differences in the PCs based on IPI, though there are qualitative differences apparent in the graphs (Fig. 3.4B). These results suggest that physiological characteristics of postsynaptic potential responses relate to whether EOD and IPI tuning results in synaptic connectivity changes in the direction predicted by the *in vitro* focal stimulation results.

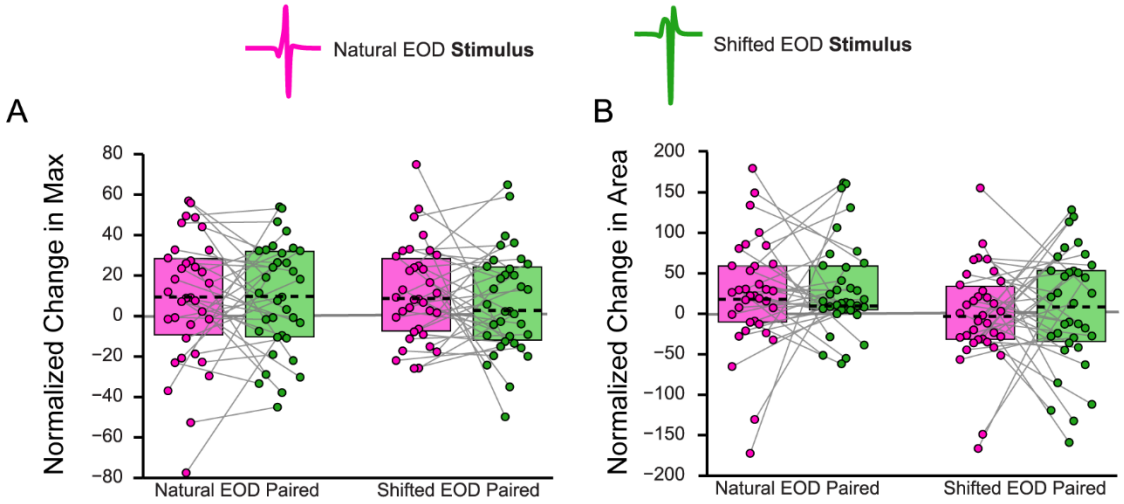

Figure 3.2. STDP does not cause changes to different EOD stimuli as predicted by *in vitro* focal stimulation data. (A) Normalized change in max values with median (black dotted line) & quartiles (boxes) for natural EODs (green, n = 35) and phase-shifted EODs (yellow, n = 25). Grey lines connect data points collected during the same trial from the same neuron. Data collected in *B. brachyistius.* (B) Same as in (A) but with normalized change in area values rather than normalized change in max values.

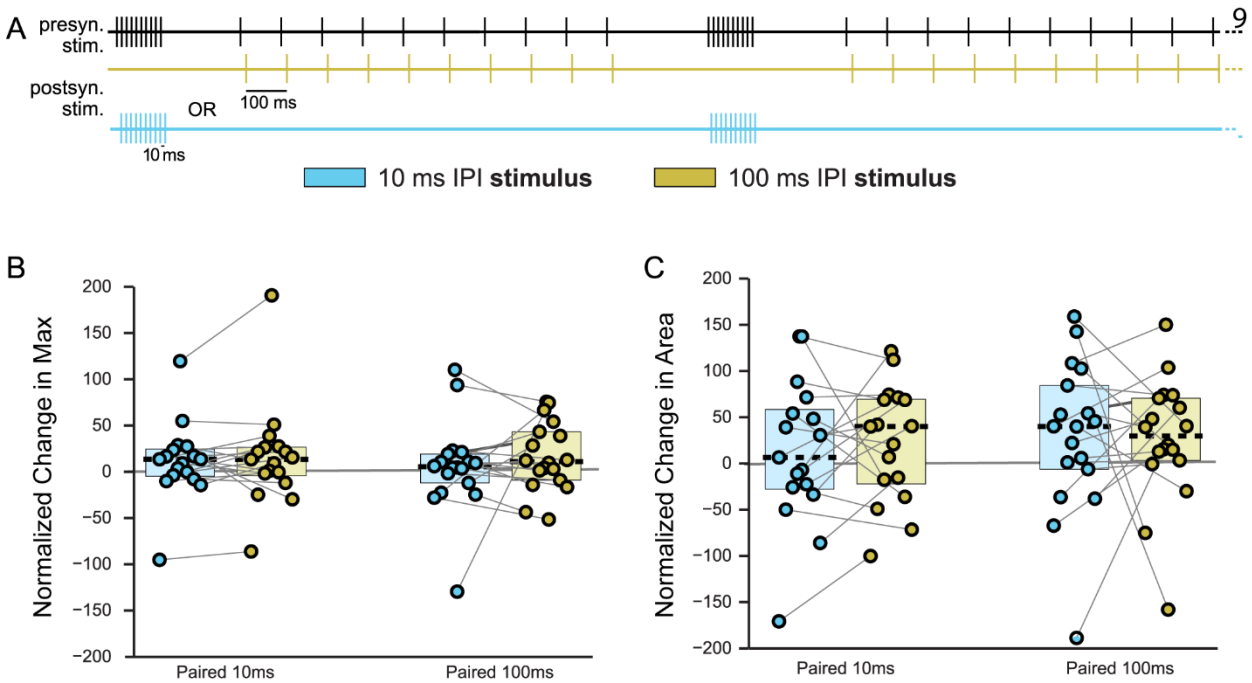

Figure 3.3. STDP does not cause changes to different IPI stimuli as predicted by *in vitro* focal stimulation. (A) Model of the stimulation protocol, showing an alternating train of 10 ms and 100 ms IPIs in black with intracellular current injection in the ELp only paired with either the 10 ms IPI (blue, n = 14) or 100 ms IPI (yellow, n = 14). (B) Normalized change in max values with median (black dotted line) & quartiles (boxes) comparing the paired IPI (paired 10 ms n = 18; paired 100 ms n = 17) to the unpaired IPI. Data collected in *B. niger*. Grey lines are connecting data points collected during the same trial in the same neuron. (C) Same as (B) but with normalized change in area values instead of normalized change in max values.

3.4 Discussion

Previous work has shown that STDP has a role in refining and altering responses to sensory input *in vivo*. In the passive and active electrosensory pathways of mormyrid fish, anti-Hebbian plasticity creates an efference copy, or 'negative image,' of predictable electrosensory input to cancel reafferent responses to self-generated input (Bell et al., 1997; Warren and Sawtell, 2016). This anti-Hebbian plasticity occurs at the synapses between granule cells and medium ganglion cells, and individual granule cells have temporally diverse responses to self-generated input, allowing for a temporally specific efference copy (Kennedy et al., 2014). This cancellation generalizes across EOD rates through EOD command rate-dependent responses of granule cells and granule cell afferents (Dempsey et al., 2019). In the functionally similar cerebellum-like dorsal cochlear nucleus (DCN) of mice, synapses from parallel fibers onto fusiform and cartwheel cells exhibit Hebbian and anti-Hebbian STDP, respectively (Fujino and Oertel, 2003; Tzounopoulos et al., 2004). More recently, cancellation of self-generated reafferent auditory input in cartwheel cells has been shown to arise through a similar plastic efference copy that is generated through anti-Hebbian STDP (Singla et al., 2017). Both of these results are clear evidence that points to an important role for STDP in sensory processing. However, these findings are specific to the adaptive filtering of self-generated reafferent sensory input. Here, I wanted to address whether STDP could play a role in altering the sensory processing of externally generated, behaviorally relevant stimuli.

In the Xenopus tadpole visual system, Hebbian STDP evoked by moving bars occurs at retinotectal synapses *in vivo*, leading to the development of motion direction tuning (Zhang et al., 1998; Engert et al., 2002; Mu and Poo, 2006). While this is clear evidence for Hebbian STDP altering sensory processing of external stimuli, these landmark studies occurred in developing

juveniles, and I was interested in sensory processing in established adult circuits. In the locust olfactory system, small assemblies of Kenyon cells encode odor. Kenyon cells synapse onto β-lobe neurons, whose synchronous activity is required for fine odor discrimination (MacLeod et al., 1998). Hebbian STDP due to odor-evoked activity in Kenyon cells and β-lobe neuron synapses helps maintain the spiking synchrony required for feed-forward information flow (Cassenaer and Laurent, 2007). In hippocampal place cells, STDP is likely involved in several processes related to spatial learning and may explain the anticipatory shifting of place fields due to experience (Mehta, 2015). These studies have explored a role for STDP in sensory processing of adult circuits, but they have shown that STDP functions to maintain or reinforce an existing sensory representation, rather than using STDP to modify responses to an actively changing sensory environment.

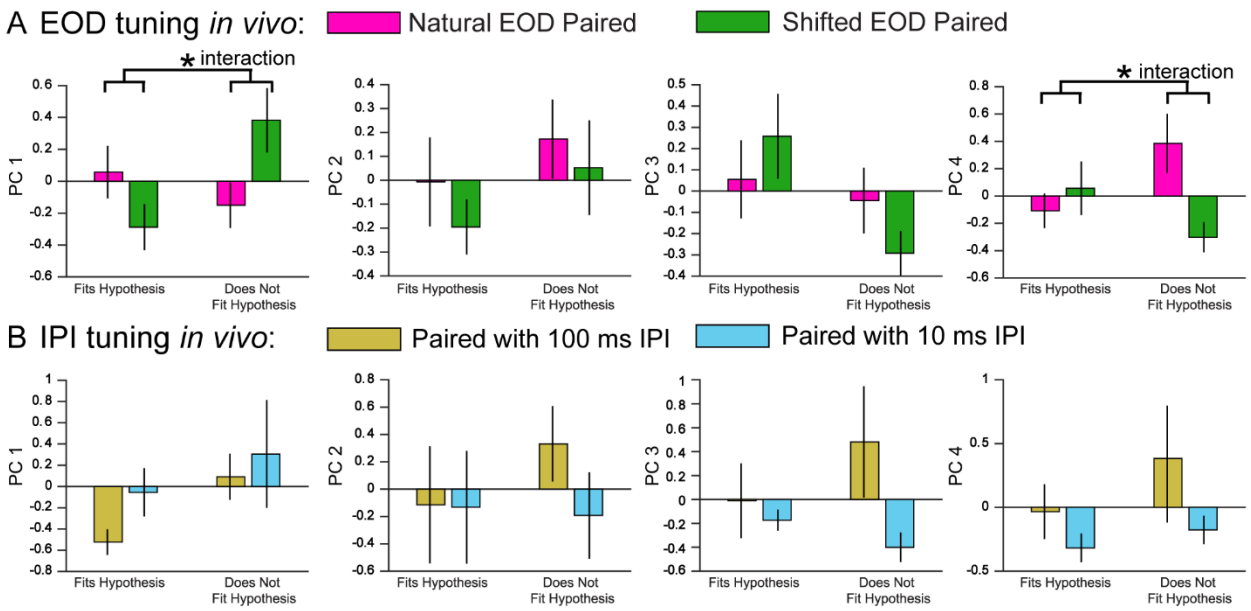

Figure 3.4. Variation in the effect of STDP on tuning is correlated with variation in synaptic responses. (A) Principal components (PC) 1-4 for the EOD tuning data that 'fits' or 'does not fit' the STDP hypothesis for natural EOD pairing (magenta) and shifted EOD pairing (green). Asterisks represent a significantly different variable or interaction stated in the text. (B) Principal components (PC) 1-4 for the IPI data that 'fits' or 'does not fit' the STDP hypothesis for both 10 ms pairing (light blue) and 100 ms pairing (yellow).

	PC 1			PC 2			PC 3			PC 4	
15.	SumTotalAreaHyp	5.59625	7.	RangeLatsDepsHyps	4.90826	5.	MedianPeak	2.53941	10.	MedianDurHyp	1.58822
4.	NumTroughs	5.42237	8.	RangelatenciesPT	4.78301	14.	MedianOnsetSlopeDep	2.48688	13.	MedianWHMinHyp	1.38176
2.	NumHyp	5.14538	8.	MedianlatenciesPT	4.17152	9.	MedianDurationDep	2.38078	12.	RangeWHMaxDep	1.02763
10.	RangeDurHyp	4.95475	7.	MedianLatsDepsHyps	3.97405	14.	MedianOffsetSlopeDep	1.95909	9.	RangeDurationDep	0.9288
13.	RangeWHMinHyp	4.80409	11.	TotalPSPDur	3.94977	15.	SumTotalAreaDep	1.70712	16.	TotalArea	0.86958
6.	RangeTrough	3.98282	3.	NumPeaks	3.555	14.	MedianOnsetSlopeHyp	1.69292	12.	MedianWHMaxDep	0.76353
14.	MedianOffsetSlopeDep	3.54589	1.	NumDep	3.55203	11.	TotalPSPDur	1.67567	11.	TotalPSPDur	0.69746
14.	RangeOnsetSlopeHyp	3.44964	9.	RangeDurationDep	2.89745	6.	MedianTrough	1.60042	15.	SumTotalAreaHyp	0.56325
10.	MedianDurHyp	3.36194	16.	TotalArea	2.57347	16.	TotalArea	1.48811	5.	RangePeak	0.52995
14.	RangeOffsetSlopeHyp	2.87186	14.	RangeOnsetSlopeDep	2.51987	13.	MedianWHMinHyp	1.37467	6.	RangeTrough	0.40773
14.	MedianOffsetSlopeHyp	2.8384	5.	RangePeak	2.21553	8.	MedianlatenciesPT	0.93956	14.	RangeOnsetSlopeDep	0.39448
13.	MedianFWHMinHyp	2.66406	4.	NumTroughs	2.11877	10.	MedianDurHyp	0.9114	3.	NumPeaks	0.39442
14.	MedianOnsetSlopeDep	2.64354	2.	NumHyp	2.10494	8.	RangelatenciesPT	0.74081	14.	RangeOnsetSlopeHyp	0.36355
16.	TotalArea	2.23949	10.	RangeDurHyp	2.0256	5.	RangePeak	0.72829	15.	SumTotalAreaDep	0.35974
11.	TotalPSPDur	2.15851	13.	RangeWHMinHyp	1.97261	7.	MedianLatsDepsHyps	0.3853	8.	RangelatenciesPT	0.34377
5.	MedianPeak	1.87024	12.	RangeWHMaxDep	1.69452	3.	NumPeaks	0.28398	9.	MedianDurationDep	0.33575
8.	RangelatenciesPT	1.58704	15.	SumTotalAreaDep	1.52029	12.	MedianWHMaxDep	0.15004	14.	RangeOffsetSlopeDep	0.30249
7.	RangeLatsDepsHyps	0.40235	14.	RangeOffsetSlopeHyp	1.385	7.	RangeLatsDepsHyps	0.13156	1.	NumDep	0.11331
8.	MedianlatenciesPT	-0.3686	14.	RangeOnsetSlopeHyp	1.32471	14.	RangeOffsetSlopeDep	0.12935	14.	MedianOffsetSlopeDep	0.11256
14.	RangeOffsetSlopeDep	-0.8762	15.	SumTotalAreaHyp	1.28519	15.	SumTotalAreaHyp	0.04955	14.	MedianOffsetSlopeHyp	0.0575
7.	MedianlLatsDepsHyps	-1.2728	6.	RangeTrough	1.20922	14.	RangeOnsetSlopeDep	0.03206	14.	MedianOnsetSlopeDep	-0.0916
9.	MedianDurationDep	-1.2911	6.	MedianTrough	0.81629	13.	RangeWHMinHyp	-0.1921	5.	MedianPeak	-0.2566
12.	MedianWHMaxDep	-1.5921	14.	RangeOffsetSlopeDep	0.69785	1.	NumDep	-0.2781	8.	MedianlatenciesPT	-0.4493
14.	MedianOnsetSlopeHyp	-2.0093	14.	MedianOnsetSlopeHyp	0.63642	14.	RangeOffsetSlopeHyp	-0.283	13.	RangeWHMinHyp	-0.4618
12.	RangeWHMaxDep	-2.0708	10.	MedianDurHyp	-0.0315	10.	RangeDurHyp	-0.346	4.	NumTroughs	-0.5279
6.	MedianTrough	-2.8896	13.	MedianWHMinHyp	-0.0756	2.	NumHyp	-0.3593	10.	RangeDurHyp	-0.545
5.	RangePeak	-3.2272	14.	MedianOffsetSlopeHyp	-0.2554	4.	NumTroughs	-0.366	2.	NumHyp	-0.6843
14.	RangeOnsetSlopeDep	-3.32	12.	MedianWHMaxDep	-0.3327	14.	MedianOffsetSlopeHyp	-0.4575	14.	RangeOffsetSlopeHyp	-0.7327
9.	RangeDurationDep	-3.3493	9.	MedianDurationDep	-1.5353	9.	RangeDurationDep	-0.7251	7.	RangeLatsDepsHyps	-0.7764
1.	NumDep	-3.699	14.	MedianOffsetSlopeDep	-1.7751	6.	RangeTrough	-1.0447	7.	MedianLatsDepsHyps	-0.9265
3.	NumPeaks	-3.8824	14.	MedianOnsetSlopeDep	-1.911	14.	RangeOnsetSlopeHyp	-1.1383	6.	MedianTrough	-1.427
15.	SumTotalAreaDep	-4.0225	5.	MedianPeak	-2.0026	12.	RangeWHMaxDep	-1.1951	14.	MedianOnsetSlopeHyp	-1.4593

Table 3.1. Synaptic potential landmarks and their respective eigenvalue loadings for PCs 1-4, referenced in Fig. 3.4A. For each PC, the loadings are ordered from largest to smallest.

	PC 1			PC 2			PC 3			PC 4	
8.	RangelatenciesPT	8.23083	15.	SumTotalAreaDep	5.08543	14.	MedianOffsetSlopeDep	2.43268	5.	MedianPeak	2.46576
11.	TotalPSPDur	8.20468	3.	NumPeaks	4.55172	14.	MedianOnsetSlopeDep	2.13523	14.	MedianOnsetSlopeDep	2.2575
7.	RangelLatsDepsHyps	7.4454	1.	NumDep	4.33446	14.	RangeOffsetSlopeHyp	2.06855	13.	MedianWHMinHyp	1.98985
16.	TotalArea	7.03629	6.	MedianTrough	4.30268	6.	RangeTrough	1.99969	14.	MedianOffsetSlopeDep	1.94976
2.	NumHyp	7.0324	14.	RangeOnsetSlopeDep	4.12122	13.	RangeWHMinHyp	1.93291	10.	MedianDurHyp	1.89372
4.	NumTroughs	6.92574	12.	RangeWHMaxDep	4.05299	5.	MedianPeak	1.79113	9.	MedianDurationDep	1.32271
8.	MedianlatenciesPT	6.64615	5.	RangePeak	4.03101	14.	MedianOnsetSlopeHyp	1.36106	8.	MedianlatenciesPT	1.16742
14.	RangeOnsetSlopeHyp	5.54792	14.	MedianOnsetSlopeHyp	3.55893	14.	RangeOnsetSlopeHyp	1.22515	11.	TotalPSPDur	0.85783
10.	RangeDurHyp	5.41251	9.	RangeDurationDep	3.12744	6.	MedianTrough	1.19559	14.	MedianOnsetSlopeHyp	0.79894
1.	NumDep	5.39284	14.	RangeOffsetSlopeDep	2.57565	10.	RangeDurHyp	0.9927	14.	MedianOffsetSlopeHyp	0.75825
7.	MedianlLatsDepsHyps	5.29467	7.	MedianLatsDepsHyps	2.19416	14.	MedianOffsetSlopeHyp	0.92961	15.	SumTotalAreaDep	0.70487
15.	SumTotalAreaHyp	5.11045	9.	MedianDurationDep	1.71783	1.	NumDep	0.7634	16.	TotalArea	0.68445
10.	MedianDurHyp	4.98317	5.	MedianPeak	1.68686	3.	NumPeaks	0.7526	8.	RangelatenciesPT	0.61123
13.	RangeWHMinHyp	4.90594	14.	MedianOnsetSlopeDep	1.60766	7.	RangeLatsDepsHyps	0.67332	6.	MedianTrough	0.44628
6.	RangeTrough	4.7513	7.	RangeLatsDepsHyps	1.51571	14.	RangeOffsetSlopeDep	0.51009	12.	MedianWHMaxDep	0.37341
3.	NumPeaks	4.56887	11.	TotalPSPDur	1.0851	14.	RangeOnsetSlopeDep	0.37461	15.	SumTotalAreaHyp	0.21988
13.	MedianWHMinHyp	4.54055	14.	MedianOffsetSlopeDep	0.93846	12.	MedianWHMaxDep	0.10458	5.	RangePeak	0.02616
14.	RangeOffsetSlopeHyp	4.2059	16.	TotalArea	0.71239	9.	MedianDurationDep	0.06534	4.	NumTroughs	-0.1585
9.	RangeDurationDep	4.20262	8.	RangelatenciesPT	0.6781	12.	RangeWHMaxDep	0.01767	14.	RangeOffsetSlopeHyp	-0.1617
14.	MedianOffsetSlopeHyp	4.05888	8.	MedianlatenciesPT	0.5859	15.	SumTotalAreaDep	0.01449	6.	RangeTrough	-0.2282
15.	SumTotalAreaDep	3.98586	13.	MedianWHMinHyp	-0.2269	7.	MedianLatsDepsHyps	-0.1881	2.	NumHyp	-0.4838
5.	RangePeak	3.93971	12.	MedianWHMaxDep	-0.6703	2.	NumHyp	-0.2613	3.	NumPeaks	-0.5931
9.	MedianDurationDep	3.69715	10.	MedianDurHyp	-0.755	16.	TotalArea	-0.4111	10.	RangeDurHyp	-0.7183
12.	RangeWHMaxDep	3.40491	13.	RangeWHMinHyp	-2.8319	4.	NumTroughs	-0.4148	13.	RangeWHMinHyp	-0.7918
14.	RangeOnsetSlopeDep	3.02775	14.	MedianOffsetSlopeHyp	-2.8526	15.	SumTotalAreaHyp	-0.5148	1.	NumDep	-0.8665
12.	MedianWHMaxDep	2.6175	4.	NumTroughs	-2.8679	8.	RangelatenciesPT	-0.5603	7.	MedianLatsDepsHyps	-0.8721
5.	MedianPeak	0.79856	14.	RangeOffsetSlopeHyp	-2.9885	5.	RangePeak	-0.6448	14.	RangeOnsetSlopeHyp	-0.9664
14.	RangeOffsetSlopeDep	0.75854	2.	NumHyp	-2.993	9.	RangeDurationDep	-0.655	14.	RangeOffsetSlopeDep	-1.0621
14.	MedianOnsetSlopeDep	0.42155	10.	RangeDurHyp	-3.1402	11.	TotalPSPDur	-0.6576	14.	RangeOnsetSlopeDep	-1.1867
14.	MedianOffsetSlopeDep	0.4129	14.	RangeOnsetSlopeHyp	-3.1511	8.	MedianlatenciesPT	-1.2964	7.	RangeLatsDepsHyps	-1.2031
6.	MedianTrough	-2.0866	6.	RangeTrough	-3.3969	10.	MedianDurHyp	-1.9792	9.	RangeDurationDep	-1.3789
14.	MedianOnsetSlopeHyp	-3.7618	15.	SumTotalAreaHyp	-3.5752	13.	MedianWHMinHyp	-1.9957	12.	RangeWHMaxDep	-1.5675

Table 3.2. Synaptic potential landmarks and their respective eigenvalue loadings for PCs 1-4, referenced in Fig. 3.4B. For each PC, the loadings are ordered from largest to smallest.

Multipolar cells exhibit the same IPI tuning to sensory stimulation as they do to direct electrical stimulation of ELa (Carlson, 2009). Despite this, while induction of STDP with presynaptic ELa focal stimulation *in vitro* generates shifts in IPI tuning consistent with Hebbian STDP (Fig 3.1), I did not find such clear results when pairing postsynaptic spiking with specific IPIs or EODs *in vivo* (Figs. 3.3 and 3.2). In addition, when we measure synaptic potential landmarks and did a PCA on those landmarks, we found significant differences in the EOD tuning data depending on whether the data did or did not 'fit' the hypothesis set by the *in vitro* data. These results suggest that physiological characteristics of postsynaptic potential responses relate to whether EOD and IPI tuning results in synaptic connectivity changes in the direction predicted by the *in vitro* focal stimulation results. Despite previous work showing the relevance of STDP in sensory processing, this disparity between *in vitro* and *in vivo* results highlights the large increase in variables that are contributing to plasticity and altering synaptic responses *in vivo* relative to *in vitro*. In conclusion, STDP is likely a relevant mechanism for shaping sensory processing, but its effects on responses to behaviorally relevant stimuli in intact organisms can be more complex than predicted by plasticity at specific synapses.

3.5 Experimental Procedures

3.5.1 Animals

In this study, I used a total of 34 *Brevimyrus niger* of both sexes, ranging from 4.5–9.4 cm in standard length and 0.8–13.5 g in mass and 40 *Brienomyrus brachyistius* of both sexes, ranging from 6.6–10 cm in standard length and 4.2–20.1 g in mass. I acquired the fish through the aquarium trade and housed them in same-species groups with a 12:12 h light/dark cycle, water conductivity

of 200–400 µS/cm, and a temperature of 25–29°C. I fed the fish live black worms four times per week. All procedures were in accordance with the guidelines established by the National Institutes of Health and were approved by the Institutional Animal Care and Use Committee at Washington University in St. Louis. *Brienomyrus brachyistius* were used for the *Brienomyrus brachyistius* specific experiment *in vitro* and for the EOD tuning experiments *in vivo*, otherwise *Brevimyrus niger* were used.

3.5.2 In vivo whole-cell recordings

I prepared fish for *in vivo* recordings from ELp as described previously (Carlson, 2009; Lyons-Warren et al., 2013b). Fish were anesthetized in 300 mg/L tricaine methanesulfonate (MS-222) and paralyzed with an intramuscular injection of 100 µl of 0.1 mg/ml gallamine triethiodide (Flaxedil). The fish was then moved to a recording chamber, where it was submerged in freshwater, except for a small region of the surface of the head. I maintained general anesthesia for surgery by respirating the fish with an aerated solution of 100 mg/ml MS-222 through a pipette tip in the mouth. The surgery site was anesthetized with 0.4% lidocaine on the skin. I then removed the skin of the surgery site, affixed a post to the skull, and removed a rectangular piece of skull covering ELp. I placed the ground electrode on the nearby cerebellum. After surgery, I brought the fish out of anesthesia by switching to aerated freshwater respiration and monitored the fish's electric organ discharge command (EODC) output with a pair of electrodes placed next to the fish's tail (Carlson, 2002, 2009; Lyons-Warren et al., 2013b; Baker et al., 2016). The EOD output is silenced by flaxedil (the muscle paralytic), but I recorded the EODC as a fictive EOD. MS-222 anesthesia silences the EODC output, so the return of EODC output indicates that the fish has recovered from anesthesia (Lyons-Warren et al., 2013b). At the end of the recording session, the respiration of the

fish was switched back to 100 mg/L MS-222 until no EODC output could be recorded, and then the fish was sacrificed by freezing.

I obtained intracellular, whole-cell patch recordings in current-clamp using previously published methods (Rose and Fortune, 1996; Carlson, 2009; Baker and Carlson, 2014). I used glass patch micropipettes with resistances of 20–40 MΩ. The pipette tip was filled with a solution (in mM) of 100 CH_3CO_2K, 2 KCl, 1 $MgCl_2$, 5 EGTA, 10 HEPES, 20 KOH, and 43 biocytin, and the pipette shank was filled with the same solution, except that biocytin was replaced with D-mannitol (Carlson, 2009; Baker and Carlson, 2014). Initial seal resistances were >1 GΩ. Recordings were amplified 10x and low-pass filtered (cutoff frequency, 10 kHz) using an Axopatch 200B amplifier (Molecular Devices), digitized at a rate of 97.7 kHz (Model RX8 Digitizer, Tucker Davis Technologies), and saved using custom software written in Matlab. I delivered electrosensory stimulation using electrodes positioned around the perimeter of the recording chamber (Lyons-Warren et al., 2013b).

3.5.3 Data collection

After patching a cell, I stimulated with bipolar square pulses, adjusting the duration (0.1–1.5 ms), intensity (3–71 mV/cm), polarity (normal or reversed), and stimulus orientation (transverse or longitudinal to the fish) to elicit maximal sub-threshold, postsynaptic potential (PSP) amplitudes from each neuron. Next, I injected intracellular, depolarizing current, adjusting the duration (1 to 8 ms) and amplitude (0.1 to 0.9 nA) until a reliable spike was produced in each neuron. All subsequent sensory and intracellular stimuli delivered during a trial then used these parameters. I did not include in the repetition count any responses to stimulus repetitions in which

stimuli occurred within 2–5 ms after an EODC response, since corollary discharge inhibition in the hindbrain blocks sensory responses within this window (Bell and Grant, 1989). I only used recordings in which the resting potential varied by 5.5 mV or less across all trials and was at least –40 mV throughout the experiment.

To explore the effect of STDP on EOD tuning, I paired post-synaptic spiking at a potentiating delay of -23 ms pre-post either with a randomly selected conspecific EOD or a 90-degree phase shifted version of that same EOD as a sensory stimulus. These EODs were randomly selected from a library of 10 EODs. I adjusted the intensity (3–71 mV/cm) and stimulus orientation (transverse or longitudinal to the fish) to elicit maximal sub-threshold, PSP amplitudes from each neuron. Both EOD sensory stimuli were repeated 20 times to get an averaged post-synaptic potential baseline response. Which EOD was paired and the order in which they were repeated was decided pseudo-randomly, to maintain an equal number of times that either a natural or phase-shifted EOD sensory stimulus was collected and to maintain an equal number of natural EOD and phase-shifted EOD pairings. One of the two EOD stimuli, pseudo-randomly selected, was paired with intracellular current injection with a -23 ms pre-post delay for 6 mins at 1 Hz. Both EOD sensory stimuli were then repeated 20 times to obtain an averaged post-synaptic potential response to compare to baseline. To measure the max of the PSP, I found the maximum point in a window from the end of the stimulus to 200 ms. In this same window, to measure the PSP area over time, I summed the post-stimulus synaptic potential trace and multiplied by one over the sampling frequency (1/sampling frequency = sampling period).

To explore the effect of STDP on IPI tuning, I paired IPI trains of sensory stimulation with intracellular spiking. I delivered two trains of sensory stimulation, the first train consisted of 10

pulses at 10 ms IPI and the second train consisted of 10 pulses at 100 ms IPI. Both IPI trains were repeated 5 times to get an averaged post-synaptic potential baseline response. During pairing, I delivered the 10 ms IPI train, followed by 450 ms of silence, then the 100 ms IPI train. While this sensory stimulation was delivered, either the 10 ms IPI train or the 100 ms IPI train was paired with 10 pulses of 10 ms IPI or 100 ms IPI postsynaptic spikes with a -23 ms pre-post delay. This pairing was repeated 300 times. The order of the pairings was decided pseudo-randomly, to maintain an equal number of times that each condition (pairing with 10 ms IPI or 100 ms IPI) was collected first. After each pairing, IPI sensory stimulation was repeated 5 times to obtain an averaged post-synaptic potential to compare to baseline. To measure the max of the PSP, I found the maximum point in a window from the end of the first stimulus in the IPI train to the start of the second stimulus in the IPI train. In this same window, to measure the PSP area over time, I summed the post-stimulus synaptic potential trace and multiplied by one over the sampling frequency (1/sampling frequency = sampling period).

3.5.4 Synaptic potential landmarks

I often observed multiple phases of depolarizations and hyperpolarizations during a post-synaptic potential. I wanted to quantify the physiological characteristics of these synaptic responses to see whether differences in those characteristics correlated with differences in the observed STDP. Synaptic potential landmarks were calculated on the pre-pairing (i.e. baseline) postsynaptic potential trace for the the EOD tuning experiments, and the first baseline postsynaptic potential in the 100 ms IPI train for the IPI tuning experiments. The raw trace was filtered with a 2 ms median filter, and the 1st and 2nd derivative were both filtered with a 5 ms zero-phase digital filter. Resting potential was calculated by averaging the 50 ms prestimulus period. The baseline

postsynaptic potential traces were zeroed by subtracting the resting potential value from the whole trace. The threshold for a depolarization or a hyperpolarization was +/- 3 standard deviations from the baseline mean, respectively. We measured 32 different landmarks from each PSP based on 16 different types of measurements. An example of a PSP illustrating these landmarks can be found in Figure 2.5. The landmarks are numbered, and the same numbers are used in Tables 3.1 and 3.2 for reference. These measurements behind these landmarks were defined and measured as follows:

1. **Total # of depolarizations**: # of points that crossed threshold with a positive slope (i.e. point (i-1) < threshold< point (i))
2. **Total # of hyperpolarizations**: # of points that crossed threshold with a negative slope (i.e. point (i-1) > threshold>point (i))
3. **Total # of peaks**: # of local maxima above threshold within a given depolarization, can be >1. The timing of each peak was also recorded. We also set a selection criterion to determine what constitutes a local maximum. We took the first derivative of the trace and recorded all the locations of sign changes in the first derivative trace. To be considered a local maximum, the peak magnitude had to be greater than the maximum value of the post-stimulus trace minus the minimum value of the post-stimulus trace, divided by 20, from above the first point of a sign change in the first derivative on either side of the peak in question (Yoder, 2022).
4. **Total # of troughs**: # of local minima below threshold within a given hyperpolarization, can be >1. The timing of each trough was also recorded. We also set a selection criterion to determine what constitutes a local minimum. We took the first derivative of the trace and recorded all the locations of sign changes in the first derivative trace. To be considered a local minimum, the trough magnitude had to be less than the maximum value of the post-stimulus

trace minus the minimum value of the post-stimulus trace, divided by 20, from below the first point of a sign change in the first derivative on either side of the trough in question (Yoder, 2022).

5. **Median and range of values of peaks:** We measured the median and range (largest peak minus smallest peak) of all the peak amplitudes.
6. **Median and range of values of troughs:** We measured the median and range (largest trough minus smallest trough) of all the trough amplitudes.
7. **Median and range of latencies to all depolarizations and hyperpolarizations**: The beginning of a depolarization was defined as the timing of the maximum in the second derivative between the end of the previous depolarization or hyperpolarization and the first peak in the depolarization. If there was no preceding hyperpolarization or depolarization, then the timing of stimulus offset was used instead. The depolarization latency was defined as the beginning of a depolarization minus the time of stimulus offset. The beginning of a hyperpolarization was defined as the timing of the minimum in the second derivative between the end of the previous depolarization or hyperpolarization and the first trough in the hyperpolarization. If there was no preceding hyperpolarization or depolarization, then the time of stimulus offset was used instead. The hyperpolarization latency was defined as the beginning of a hyperpolarization minus the time of stimulus offset. The median and range were calculated for all the depolarization and hyperpolarization latencies combined.
8. **Median and range of latencies to all peaks and troughs**: The peak latency was defined as the timing of the peak minus the timing of stimulus offset. The trough latency was defined as the timing of the trough minus the timing of stimulus offset. The median and range were calculated for all the peak and trough latencies combined.

9. **Median and range of total duration of each depolarization**: Peaks in the second derivative were defined the same as peaks in the PSP (see above), but on the 2nd derivative trace (Yoder, 2022). The end of a depolarization was defined as the timing of the first peak in the second derivative after the offset threshold crossing used to define the depolarization. End latency was defined as the end of a depolarization minus the timing of stimulus offset. The total duration of the depolarization was defined as the depolarization end latency minus the depolarization latency. The median and range were calculated for all the depolarization durations.
10. **Median and range of total duration of each hyperpolarization**: Troughs in the second derivative were defined the same as troughs in the PSP (see above), but on the 2nd derivative trace (Yoder, 2022). The end of a hyperpolarization was the time of the first trough in the second derivative after the offset threshold crossing used to define the hyperpolarization. End latency was defined as the end of a hyperpolarization minus the timing of stimulus offset. The total duration of the hyperpolarization was defined as the hyperpolarization end latency minus the hyperpolarization latency. The median and range were calculated for all the hyperpolarization durations.
11. **Total PSP duration**: Total PSP duration was defined as the end latency of the last depolarization/hyperpolarization minus the first depolarization/hyperpolarization latency.
12. **Median and range of duration at half max value of each depolarization**: First, we found the value at half of the max, which is the largest peak of a depolarization plus the magnitude at the depolarization latency, divided by two. Then, we found the timings of half max before and after the largest peak. The duration at half max equaled the timing of half max after peak minus the timing of half max before peak.

13. **Median and range of duration at half min value of each hyperpolarization**: First, we found the value at half of the min, which is the largest trough of a hyperpolarization plus the magnitude at the hyperpolarization latency, divided by two. Then, we found the timings of half min before and after the largest trough. The duration at half min equaled the timing of half min after trough minus the timing of half min before trough.
14. **Median and range of onset and offset average slope of depolarizations and hyperpolarizations**: The depolarization onset slope was calculated by taking the largest peak magnitude of a depolarization minus the depolarization start magnitude, divided by the difference of time between those two points. The hyperpolarization onset slope was calculated by taking the largest trough magnitude of a hyperpolarization minus the hyperpolarization start magnitude, divided by the difference in time between those two points. The depolarization offset slope was calculated by taking the largest peak magnitude of a depolarization minus the depolarization end magnitude, divided by the difference in time between those two points. The hyperpolarization offset slope was calculated by taking the largest trough magnitude of a hyperpolarization minus the hyperpolarization end magnitude, divided by the difference in time between those two points.
15. **Summed area of depolarizations and hyperpolarizations**: The depolarizations area was calculated by summing all values above threshold then multiplying by multiplied by one over the sampling frequency (1/sampling frequency = sampling period). The hyperpolarizations area was calculated by summing all values below threshold and then multiplying by multiplied by one over the sampling frequency (1/sampling frequency = sampling period)
16. **PSP total area**: The total area was calculated by summing the total depolarizations area (from above) and the hyperpolarizations area (from above).

3.5.5 Experimental design and statistical analyses

The goal of this study was to explore the role of STDP in shaping sensory tuning. To do this I performed experiments in mormyrid weakly electric fish to take advantage of a sensory system in which I could precisely stimulate a sensory system both *in vitro* and *in vivo* in a behaviorally relevant way in an intact circuit. The details of the stimulations are stated above for each particular experiment. Unless otherwise stated, values are represented as median and 75%/25% quartiles. The Area and Max calculations were normalized by subtracting the after minus before value and dividing by the absolute value of the maximum of the after and before, multiplied by 100. A two-way ANOVA was used to compare the stimulus*pairing interactions. A Bonferroni correction for multiple comparisons was used unless otherwise stated. Details of the synaptic landmark measurements are found in the section above entitled Synaptic potential landmarks. A principal components analysis was performed on the landmarks measured. The first four principal components were retained for each. Statistical analysis was done in SPSS and Matlab.

3.6 Acknowledgements

I thank Xiaofeng Ma for completing the *in vitro* experiments that led to this work. Funded by NSF IOS 1755071.

CHAPTER 4

Intrinsic firing patterns in a network due to sensory stimulus repetition does not alter sensory tuning *in vivo* or behavioral sensitivity

Authors:

Adalee Lube, Bruce A. Carlson

Author affiliations:

Department of Biology, Washington University in Saint Louis, MO, 63130, USA

4.1 Abstract

I addressed how intrinsic network activity could alter synaptic and behavioral responses *in vivo*. Spike-timing-dependent plasticity (STDP) is one of the leading frameworks for how neural connectivity changes within learning and memory (Markram et al., 1997; Song et al., 2000; Bi and Poo, 2001; Feldman, 2012). However, precise experimental demonstration of STDP generally requires artificially inducing post-synaptic spiking. In a naturalistic setting, it is less likely that a precisely timed post-synaptic spike invariably follows the presynaptic neuronal response to a sensory stimulus. Here, I asked how intrinsic patterns of firing in a network triggered by sensory stimulus repetition could drive changes in synaptic responses to that stimulus. I explored this question using *in vivo* electrophysiology and behavior experiments in mormyrid weakly electric fish, which enables the use of ethologically relevant stimuli to stimulate central sensory neurons with the same temporal patterns from presynaptic stimulation *in vitro* or sensory stimulation *in vivo*. First, in extracellular evoked potential recordings in the midbrain anterior and posterior exterolateral nuclei (ELa and ELp, respectively), I recorded local field potentials before and after repetition of a sensory stimulus. Second, in a freely behaving recording paradigm, I recorded electric organ discharge (EOD) rate before and after repetition of a sensory stimulus. Neither set of experiments revealed a statistically significant effect of sensory repetition. Although I previously found that STDP induced by post-synaptic spiking could alter sensory responses *in vivo*, I did not observe a significant change in sensory responses resulting from sensory repetition alone. This discrepancy, taken together with abundant *in vitro* support for STDP, suggests that although STDP could be a mechanism for altering sensory tuning in a natural environment, there are likely other processes and mechanisms that work in conjunction to provide tuning adaptation.

4.2 Introduction

The majority of work surrounding the relevance of STDP to *in vivo* sensory processing relies on artificially induced post-synaptic spiking (Feldman, 2012). In addition to experiments with artificially induced post-synaptic spiking, elegant studies of *stimulus*-timing-dependent-plasticity (rather than *spike*-timing-dependent-plasticity) have shown that the relative-timing of multiple sensory stimuli evoked changes in sensory tuning (Dan and Poo, 2004; Shulz, 2010). In cat visual cortex, repetitive pairing of two visual stimuli at different orientations induced a change in the orientation tuning of visual cortical neurons that was dependent on the temporal order of the orientations presented (Yao and Dan, 2001). In the primary auditory cortex of adult ferrets, repetitive pairing of tones of different frequencies induced shifts in neuronal frequency selectivity (Dahmen et al., 2008). In general, previous studies focused on the repetitive pairing of sensory stimuli within the temporal window associated with STDP. However, I was interested in whether intrinsic patterns of firing in a network due to repetition of a sensory stimulus could alter sensory responses, without restricting the stimulus to a pairing within a narrow window of time. Indeed, previous work done in mormyrid weakly electric fish (Ma and Carlson, unpublished; Fig. 4.1), using intracellular recordings in a whole-brain *in vitro* preparation, has shown that repetition of a presynaptic stimulus train with a particular inter-pulse interval (IPI) showed a selective potentiation in the neuronal responses to the repeated IPI (Figure 4.1).

Because I was interested in changes occurring across a network, I did extracellular local field potentials recordings in the ELa and ELp. These local field potentials, called evoked potentials, represent summed electrical activity from multiple neurons near the recording electrode. In addition to electrophysiology, I was also interested in how sensory stimulus repetition could alter behavioral output. Previous work has shown that fish have greater behavioral sensitivity

to stimuli that elicit greater responses among ELp multipolar cells (Lyons-Warren et al., 2012; Baker et al., 2016). I wanted to explore whether sensory stimulus repetition, without paired intracellular spiking, could alter both ELa and ELp sensory responses *in vivo* and behavioral output.

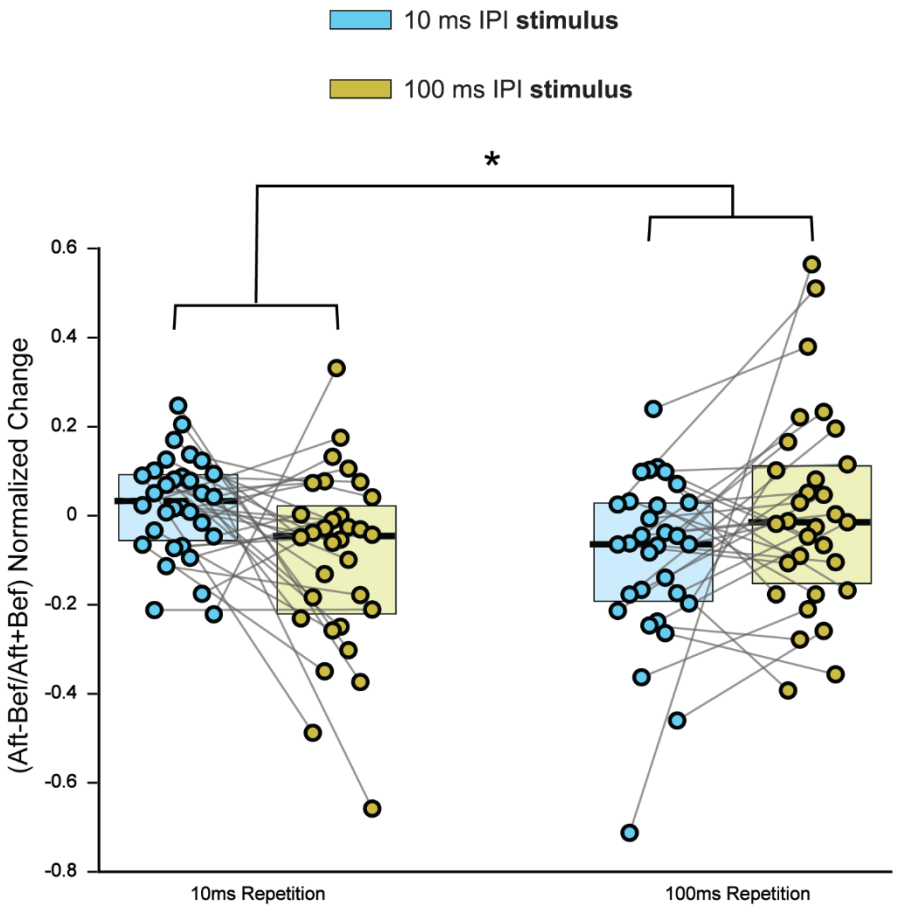

Figure 4.1. ELa presynaptic stimulus repetition alters IPI tuning *in vitro*. Normalized change in EPSP amplitude with median (black dotted line) & quartiles (boxes) for the paired IPI (paired 10 ms n = 32; paired 100 ms n = 31) to the unpaired IPI. Data collected in *B. niger*. Grey lines are connecting data points collected during the same trial in the same neuron. Two-way repeated measures ANOVA p = 0.003 stimulus*pairing interaction.

4.3 Results

4.3.1 EOD sensory stimulus repetition did not alter synaptic responses to different EOD stimuli

I sought to determine whether sensory responses could be altered *in vivo* in response to repetition of an EOD sensory stimulus. In the mormyrid weakly electric fish, the midbrain ELa is tuned to EOD waveform (Xu-Friedman and Hopkins, 1999; Lyons-Warren et al., 2013a) and the ELp is tuned to waveform and inter-pulse-interval (IPI) (Carlson, 2009; Baker et al., 2013), so any change in the EOD tuning could occur in either the ELa or the ELp. In these experiments in *Brevimyrus niger*, I provided presynaptic input using sensory stimulation while recording extracellular evoked potentials simultaneously from the ELa and the ELp. The sensory stimuli consisted of a conspecific EOD and a 90-degree phase shifted version of the same EOD, randomly selected from a library of conspecific EODs. During repetition, the version of the EOD to be repeated was pseudo-randomly decided and then repeated for 6 minutes at 1 Hz. Evoked potential responses were collected before and after repetition for both EOD stimuli at intensities from 0.5 to 293.9 mV/cm. I measured the peak-to-peak (maximum-to-minimum) value of the evoked potential responses before and after the repetition, and these peak-to-peak values were normalized using the sum of the after and before peak-to-peak values divided by the difference of after minus before. I analyzed the differences in the data across the 3 independent variables, including whether the value was from the repeated or control EOD, from a natural or phase-shifted EOD, and what intensity the data was collected from. Using a three-way repeated measure ANOVA, I found no significant differences in the data due to these conditions, nor any significant interactions (Fig 4.2).

4.3.2 IPI sensory stimulus repetition potentiated synaptic responses to a short IPI only

I sought to determine whether sensory responses could be altered *in vivo* in response to repetition of an IPI sensory stimulus. In these experiments in *Brevimyrus niger*, I provided presynaptic input using sensory stimulation while recording extracellular evoked potentials from the ELp. The sensory stimuli consisted of a train of 10 pulses with a 10 ms inter-pulse interval and a train of 10 pulses with a 100 ms inter-pulse interval. During repetition, the IPI train to be repeated was randomly decided and then was repeated 300 times. Evoked potential responses were collected before and after repetition for both IPI stimuli. Using a two-way repeated measure ANOVA, I found a significant effect of IPI stimulus only ($p = 0.02$) (Fig 4.3).

4.3.3 EOD sensory stimulus repetition did not alter behavioral output

Next, I explored how sensory stimulus repetition would affect behavioral output. In a freely behaving, established playback and recording preparation (Carlson et al., 2011; Lyons-Warren et al., 2012; Baker et al., 2015, 2016), I recorded EOD rate output in an experimental design similar to the EOD stimulus repetition design for the evoked potential recordings described in section 4.3.1. The sensory stimuli consisted of a conspecific EOD and a 90-degree phase shifted version of the same EOD, randomly selected from a library of conspecific EODs. During repetition, the version of the EOD to be repeated was randomly decided and then repeated for 6 minutes at 1 Hz. The repetition was done at either of two intensities, 131.5 mV/cm or 13.15 mV/cm, also decided pseudo randomly. EOD rate output was recorded before and after repetition for both EOD stimuli at intensities from 0.8 to 13.15 mV/cm. I measured the max – mean EOD rate for each intensity and EOD type. To account for individual variance in EOD rate across individuals, I normalized the data by taking the max minus the baseline mean and dividing by the baseline standard

deviation. Using a three-way repeated measure ANOVA, I found no significant differences in the data due to any of the independent variables nor any significant interactions (Fig 4.4).

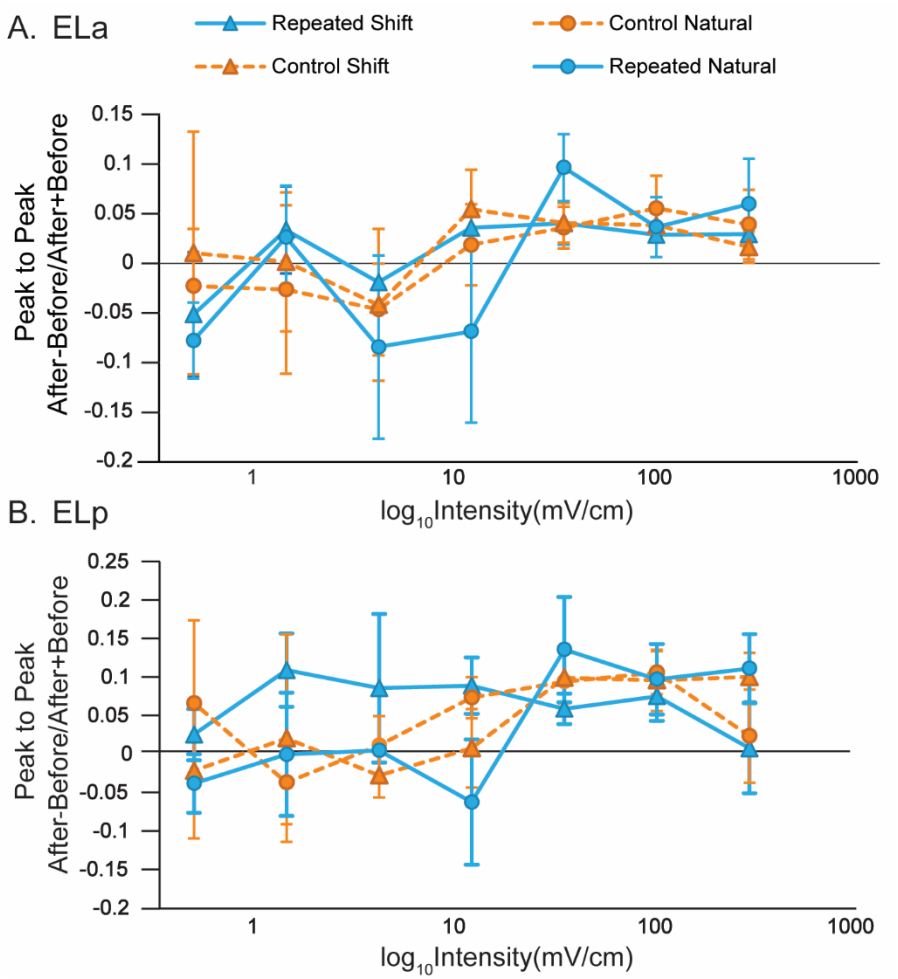

Figure 4.2. EOD sensory stimulus repetition does not alter EOD tuning *in vivo* in ELa or ELp. (A) ELa normalized change in peak-to-peak evoked potential amplitude across seven intensities with average values for shifted EODs marked with a triangle and natural EODs marked with a circle. The blue solid line marks the repeated EOD and the orange dotted line marks the control EOD (repeated n = 9; control n = 8). Error bars represent standard error of the mean (SEM). (B) ELp normalized change in peak-to-peak evoked potential amplitude across seven intensities with average values for shifted EODs marked with a triangle and natural EODs marked with a circle. The blue solid line marks the repeated EOD and the orange dotted line marks the control EOD (repeated n = 9; control n = 8). Error bars represent standard error of the mean (SEM). Data collected in *B. niger*.

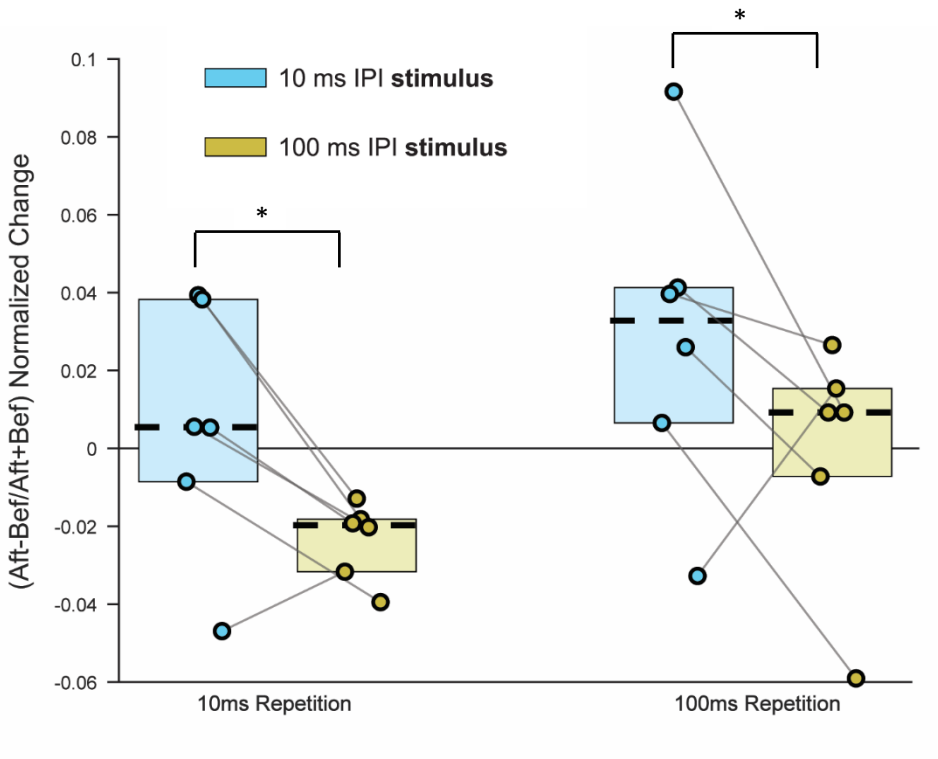

Figure 4.3. IPI train sensory stimulus repetition responses to 10 ms IPIs *in vivo*. Normalized change in peak-to-peak evoked potential amplitude with median (black dotted line) & quartiles (boxes) for the paired IPI (paired 10 ms n = 6; paired 100 ms n = 6) to the unpaired IPI. Data collected in *B. niger*. Grey lines are connecting data points collected during the same trial in the same neuron. Two-way repeated measures ANOVA p = 0.02 for IPI stimulus only.

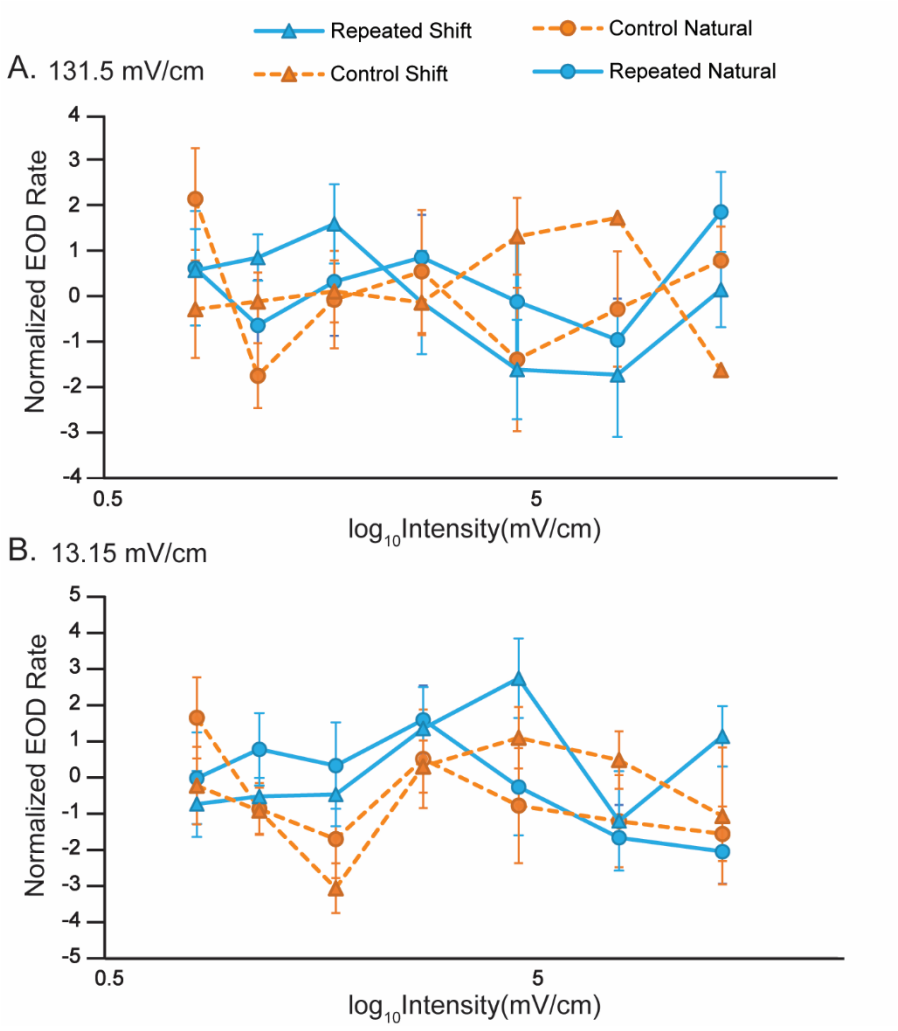

Figure 4.4. EOD sensory stimulus repetition does not alter EOD output rate *in vivo*. (A) 131.5 mV/cm repetition intensity normalized change in EOD rate across seven intensities with average values for shifted EODs marked with a triangle and natural EODs marked with a circle. The blue solid line marks the repeated EOD and the orange dotted line marks the control EOD (repeated n = 17; control n = 17). Error bars represent standard error of the mean (SEM). (B) 13.15 mV.cm repetition intensity normalized change in EOD rate across seven intensities with average values for shifted EODs marked with a triangle and natural EODs marked with a circle. The blue solid line marks the repeated EOD and the orange dotted line marks the control EOD (repeated n = 17; control n = 17). Error bars represent standard error of the mean (SEM). Data collected in *B. brachyistius*.

4.4 Discussion

Previous studies employing intracellular, whole cell recordings in mormyrid weakly electric fish *in vitro* showed that repetition of a presynaptic stimulus train with a particular IPI was enough to potentiate the central sensory neuron responses to the repeated IPI (Ma and Carlson, unpublished; Fig 4.1). Rather than artificially induce postsynaptic spiking to study a synaptic strength, I wanted to explore how presynaptic sensory stimulation would alter sensory neuron responses to sensory stimulus repetition alone *in vivo*. Because I was interested in how patterns of firing in a network could alter sensory responses, I repeated a similar stimulation paradigm to the *in vitro* work described above, in extracellular evoked potential recordings *in vivo* to capture the collective activity of more neurons than intracellular recordings. *In vivo*, I observed a selective increase in evoked potential responses for each of the 10 ms IPI stimuli, independent of which IPI was repeated. With an N = 6, I will likely be doing a few more experiments to see if this trend holds. In addition to using IPI sensory repetition, I also used EOD sensory repetition. For these experiments, I recorded extracellularly, simultaneously from both the ELa and the ELp, since both areas are tuned to EOD waveform (Xu-Friedman and Hopkins, 1999; Baker et al., 2013; Lyons-Warren et al., 2013a) and I did not want to exclude the possibility that sensory repetition could alter responses in either area. I did not find a change in the sensory responses that was specific to the repeated EOD in either the ELa or the ELp.

Due to the differences in neural activity patterns in the ELa/ELp present *in vitro* and *in vivo*, one of the goals of these experiments was to determine if the same pattern of presynaptic input could induce similar changes to neuronal responses *in vitro* and *in vivo*. I found that a repetition of the same stimulus, repetition frequency and repetition amount of time *in vitro* or *in vivo* did not induce similar sensory responses. To address this discrepancy, the next step would be

to probe the different dynamics of altering sensory responses *in vivo*. Experiments can be done systematically varying the repetition intensity of sensory stimuli, the length of repetition time and the frequency of the sensory stimulus during the repetition to explore which sensory stimulus parameters induce changes in the sensory neuron responses. Prior work has shown that the dynamics of stimuli that successfully alter sensory neuron responses differ between *in vitro* and *in vivo* conditions (Shulz, 2010). Studying STDP in the somatosensory cortex of the rat, Jacob et al., (Jacob et al., 2007) showed that the post-leads-presynaptic pairing led to synaptic depression when the postsynaptic spiking occurred less than 17 ms before the presynaptic input, which is a narrower window for STDP than previously observed *in vitro* (Feldman, 2000, 2012). In the cat visual cortex *in vivo*, by pairing a visual stimulus with electrical cortical stimulation within the standard STDP window, Schuett et al. (Schuett et al., 2001) showed that sensory-preceding-electrical stimulation induced an enhanced cortical response to the visual stimulus, whereas electrical-preceding-sensory stimulation resulted in a reduced cortical response to the visual stimulus. These changes were found to last for 18 hours, but the pairing protocol itself lasted for 3 - 4 hours at 7 Hz (resulting in around 25,000 pre-and postsynaptic pairings), which is substantially longer and more intense than is typically employed in the field.

Using a similar paradigm to the EOD tuning experiments above, I recorded behavioral (EOD rate) output to a conspecific EOD stimulus and a phase shifted EOD stimulus before and after repetition of one of the EOD stimuli. I found no change in the EOD that was specific to the repeated stimuli. I did a set of experiments with the repetition intensity at 131.5 mV/cm and a set of experiments with the repetition intensity at 13.15 mV/cm. There was no difference in the outcome between the two repetition intensities. The repetition frequency and time was 1 Hz for 6 mins for both experiments. Despite finding that sensory stimulus repetition did not induce change

in sensory neuron or behavioral responses, these results did show that the induction dynamics of potentiation and depression *in vitro* do not always transfer *in vivo*. This motivates future work that more systematically characterizes the parameter space of sensory stimulus dynamics in terms of efficacy of altering sensory tuning *in vivo* via sensory stimulus repetition.

4.5 Experimental Procedures

4.5.1 Animals

In this study, I used a total of 11 *Brevimyrus niger* of both sexes, ranging from 5–8.3 cm in standard length and 34 *Brienomyrus brachyistius* of both sexes, ranging from 7–12.8 cm in standard length. The Carlson lab acquired the fish through the aquarium trade and housed them in same-species groups with a 12:12 h light/dark cycle, water conductivity of 200–400 µS/cm, and a temperature of 25–29°C. The fish were fed live black worms or frozen blood worms four times per week. All procedures were in accordance with the guidelines established by the National Institutes of Health and were approved by the Institutional Animal Care and Use Committee at Washington University in St. Louis.

4.5.2 *In vivo* evoked potential recording

I prepared fish for *in vivo* recordings from ELa and ELp as described previously (Carlson, 2009; Lyons-Warren et al., 2013b). Fish were anesthetized in 300 mg/L tricaine methanesulfonate (MS-222) and paralyzed with an intramuscular injection of 100 µl of 0.1 mg/ml gallamine triethiodide (Flaxedil). The fish was then moved to a recording chamber, where it was submerged in freshwater, except for a small region of the surface of the head. I maintained general anesthesia for surgery by respirating the fish with an aerated solution of 100 mg/ml MS-222 through a pipette tip in the mouth. The surgery site was anesthetized with 0.4% lidocaine on the skin. I then removed

the skin of the surgery site, affixed a post to the skull, and removed a rectangular piece of skull covering ELp. I placed the ground electrode on the nearby cerebellum. After surgery, I brought the fish out of anesthesia by switching to aerated freshwater respiration and monitored the fish's electric organ discharge command (EODC) output with a pair of electrodes placed next to the fish's tail (Carlson, 2002, 2009; Lyons-Warren et al., 2013b; Baker et al., 2016). The EOD output is silenced by flaxedil (the muscle paralytic), but I recorded the EODC as a fictive EOD. MS-222 anesthesia silences the EODC output, so the return of EODC output indicates that the fish has recovered from anesthesia (Lyons-Warren et al., 2013b). At the end of the recording session, the respiration of the fish was switched back to 100 mg/L MS-222 until no EODC output could be recorded, and then the fish was sacrificed by freezing.

I recorded evoked potentials in the ELa and ELp, done as previously described (Carlson, 2009; Lyons-Warren et al., 2013b), using electrodes made of borosilicate capillary glass (o.d. = 1.0 mm, i.d. = 0.5 mm; A-M Systems, Model 626000) pulled on a Flaming/Brown micropipette puller (Sutter Instrument Company model P-97), broken to a tip diameter of 10–15 mm, and filled with 3M NaCl. Recordings of evoked potentials were obtained after the fish had completely recovered from anesthesia. Evoked potentials were amplified 1000x and band-pass filtered (0.01–5 kHz) with a differential AC amplifier (A-M systems, Model 1700), digitized at a rate of 97.6 kHz (Tucker Davis, Model RX 8), and saved using custom software in Matlab.

4.5.3 Evoked potential data collection

After finding evoked potentials in the ELa and ELp simultaneously, to explore the effect of sensory stimulus repetition on EOD tuning, I repeated either a randomly selected conspecific EOD or a 90-degree phase shifted version of that same EOD. These EODs were randomly selected from a library of 10 EODs. All EOD sensory stimuli were repeated 20 times to get an averaged

evoked potential baseline response at a range of seven intensities from 0.5 to 293.9 mV/cm, ordered decided randomly. I did not include in the repetition count any responses to stimulus repetitions in which stimuli occurred within 2–5 ms after an EODC response, since corollary discharge inhibition in the hindbrain blocks sensory responses within this window (Bell and Grant, 1989). Which EOD was repeated and the order in which they were repeated was decided pseudo-randomly, to maintain an equal number of an equal number of natural EOD and phase-shifted EOD pairings. One of the two EOD stimuli, pseudo-randomly selected, was repeated for 6 mins at 1 Hz. All EOD sensory stimuli were then repeated 20 times to obtain an averaged evoked potential response to compare to baseline. I then measured the peak-to-peak value of the evoked potential response post-stimulus artifact.

To explore the effect of sensory stimulus repetition on IPI tuning, I repeated IPI trains of sensory stimulation. I delivered two trains of sensory stimulation, the first train consisted of 10 bipolar square pulses at 10 ms IPI and the second train consisted of 10 bipolar square pulses at 100 ms IPI. Both IPI trains were repeated 10 times to get an averaged post-synaptic potential baseline response. During repetition, I delivered either the 10 ms IPI train or the 100 ms IPI train 300 times. The order of the pairings was decided pseudo-randomly, to maintain an equal number of times that each condition (pairing with 10 ms IPI or 100 ms IPI) was collected first. After each pairing, IPI sensory stimulation was repeated 10 times to obtain an averaged post-synaptic potential to compare to baseline. I then measured the peak-to-peak value of the evoked potential response post-stimulus artifact.

4.5.4 Behavioral playback experiments

To test behavioral responses to sensory stimulus repetition, we recorded the EOD output of a fish during the presentation of natural and phase-shifted EODs using previously described

methods (Carlson et al., 2011; Lyons-Warren et al., 2012). We placed a rectangular plastic chamber (4.1 x 4.1 x 20.3 cm) in the middle of a small behavior tank filled with home tank water. Most fish entered the chamber voluntarily within five minutes. If fish were not within the chamber after 5 min, we guided fish into the chamber with a net. Netted caps were placed over each end of the chamber to keep the fish inside during the experiment. Fish were then allowed an additional 10 min to acclimate to the chamber. A pair of Ag/AgCl electrodes oriented horizontally on both sides of the chamber delivered the stimulus, and a pair of Ag/AgCl electrodes oriented vertically on both ends of the chamber recorded the EOD output of the fish. I repeated either a randomly selected conspecific EOD or a 90-degree phase shifted version of that same EOD. These EODs were randomly selected from a library of 10 EODs. All EOD sensory stimuli were repeated 20 times to get an averaged baseline EOD output at a range of seven intensities from 0.5 to 13.15 mV/cm, ordered decided randomly. Which EOD was repeated and the order in which they were repeated was decided pseudo-randomly, to maintain an equal number of an equal number of natural EOD and phase-shifted EOD repetitions. One of the two EOD stimuli, pseudo-randomly selected, was repeated for 6 mins at 1 Hz. All EOD sensory stimuli were then repeated 20 times to obtain an averaged EOD output to compare to baseline. All stimuli were generated in Matlab 7 (MathWorks), digital-to-analog converted at a rate of 97.7 kHz (RX8, Tucker-Davis Technologies), and attenuated (PA5, Tucker-Davis Technologies) before delivery to an analog stimulus isolator (Model 2200, A-M Systems) connected to the stimulus electrodes. To record the EOD output of a fish, we amplified electrical activity 100 times with bandpass filtering (0.1 Hz–20 kHz; Model 1700, A-M Systems), recorded EOD times as events that crossed a manually set threshold, and then saved these times using custom software in Matlab. We computed the spike density function (SDF) by convolving each EOD time of occurrence with a Gaussian of 200 ms

width (Carlson and Hopkins, 2004), and then averaging over stimulus presentations. We measured the baseline EOD rate of the fish by averaging the SDF over a window starting 0.2 s after the start of a 5s prestimulus period and ending 0.2 s before stimulus onset. We measured the maximum EOD rate that occurred in a window starting 0.1 s before stimulus onset up to 2.1 s after stimulus offset. The response window started before stimulus onset since the Gaussian used in the convolution was symmetric in time, such that a response immediately following stimulus onset could affect the SDF for up to 100 ms (i.e., half-width of the Gaussian) before the stimulus. The EOD rate response was defined by subtracting the baseline EOD rate from the maximum EOD rate.

4.6 Acknowledgements

I thank Xiaofeng Ma for completing the *in vitro* experiments that led to this work. Funded by NSF IOS 1755071.

CHAPTER 5

Conclusions

5.1 Introduction

In this dissertation, I used mormyrid electric fishes to study the role of spike-timing-dependent-plasticity (STDP) in real-time sensory tuning adaptation in adult organisms *in vivo*. Previous work in mormyrids found that Hebbian STDP predictably alters sensory tuning *in vitro* with focal presynaptic stimulation (Ma and Carlson, unpublished; Fig. 1.1). First, I studied how sensory responses could be altered by a similar Hebbian STDP paradigm *in vivo*. I found that STDP does alter midbrain synaptic responses to sensory stimuli *in vivo*, but that the change in responses due to STDP to not always follow the STDP rules established *in vitro* (Chapter 2). Next, I found that STDP did not alter sensory tuning to conspecific electric organ discharge (EOD) stimuli or to inter-pulse interval (IPI) stimuli (Chapter 3). However, after measuring synaptic potential landmarks and performing a PCA analysis on those landmarks, I found significant differences in the PC scores depending on whether the data did or did not 'fit' the hypothesis established by previous experiments *in vitro* (Chapters 2 and 3). Because the landmarks were measurements of the different positive and negative components in a postsynaptic potential, significant differences in the PC scores due to 'fit' suggests that differences in the presence of inhibition and polysynaptic activity in a post-synaptic potential effected how well the data 'fit' the hypothesis established from *in vitro* results (Chapters 2 and 3). Because a large postsynaptic spike likely does not follow every single neuronal response to sensory stimuli in real-time tuning adaptation *in vivo*, I explored how sensory stimulation alone would alter both midbrain neuron responses and behavioral output *in vivo*. I found that there was no significant change in sensory neuron responses or behavior due to a sensory stimulus repetition with the same repetition time and frequency as was done with induced postsynaptic spiking previously (Chapter 4). With mormyrids, I have investigated STDP, a highly studied mechanism for altering synaptic strength,

in the context of sensory tuning *in vivo*. My findings suggest that STDP rules operating at identified synapses *in vitro* may not drive predictable changes in sensory responses at the circuit or behavior level.

5.2 The differences found in sensory tuning *in vivo*, compared to *in vitro*

Previous work done in the posterior exterolateral nucleus (ELp) of mormyrids in a whole brain preparation with focal postsynaptic stimulation *in vitro* showed that that there was an increase in the synaptic strength for pre-leads-post synaptic delays and a decrease in the synaptic strength for post-leads-presynaptic delays, a Hebbian STDP pattern (Ma and Carlson, unpublished; Fig. 1.1) and that STDP could alter inter-pulse interval (IPI) sensory tuning *in vitro* in the ELp (Ma and Carlson, unpublished; Fig. 3.1). These results suggested that STDP was a viable mechanism for altering IPI sensory tuning *in vivo* as well, especially due to the unique advantages of studying STDP in mormyrids. The complex relationship between sensory stimuli and the resulting patterns of synaptic input to central sensory neurons makes bridging the gap between STDP observed *in vitro* and its relevance to sensory processing and behavior *in vivo* complicated. Since the properties of neuronal activity patterns differ between *in vitro* and *in vivo* preparations, I explored if STDP exhibits similar induction requirements between the two. With mormyrids, I can induce the same behaviorally relevant patterns of presynaptic activity *in vivo* that were used in experiments *in vitro*. This is because anterior exterolateral nucleus (ELa) output, the presynaptic input to the ELp, precisely follows the timing of electric sensory stimulus pulses (Hopkins and Bass, 1981; Lyons-Warren et al., 2013a). Thus, my initial hypothesis was that STDP would also alter sensory tuning in a similar manner as was found *in vitro*. Surprisingly, my dissertation showed that although STDP can alter synaptic responses to sensory stimuli *in vivo* (Chapter 2), the STDP pattern was not as clear as found with focal presynaptic stimulation *in vitro* (Chapter 2).

A given EOD stimulates a distinct subpopulation of cells in the ELa (Baker et al., 2013; Lyons-Warren et al., 2013a) and the ELa provides topographic, excitatory input to the ELp (Friedman and Hopkins, 1998). Because excitatory ELp-to-ELp connections tend to occur over short distances (Ma et al., 2013), sensory stimulation would activate focal ELa inputs that provide direct excitatory input to the recorded neuron and adjacent ELp neurons, as well as excitatory input to more distant ELp neurons (Xu-Friedman and Hopkins, 1999) and thus would be expected to stimulate more inhibitory inputs to recorded neurons compared to pathways excited by focal ELa stimulation. Experiments *in vitro* were also done using an array of stimulus electrodes to stimulate presynaptically, rather than a single, focal stimulus electrode. When postsynaptic ELp spikes were paired with presynaptic stimulation using an electrode array in ELa (Fig. 1.2B), at pre-leads-post or post-leads-pre delays, both potentiation and depression were observed (Fig. 1.2B). These results show that stimulating a larger, more diffuse population of ELa neurons can result in a more variable pattern of STDP as compared to focal ELa stimulation.

5.3 Future Directions

Recruitment of more inhibitory pathways to the recorded neurons likely contributed to the differences observed between focal presynaptic stimulation results *in vitro* and sensory presynaptic stimulation results *in vivo*, but there are additional factors that are worth exploring as future directions. In all experiments, presynaptic stimulation and postsynaptic spiking were paired for 6 minutes at 1 Hz. A known mechanism of long-term potentiation and depression is stimulation/pairing rate, but there is also an interaction between stimulus rate and timing for STDP specifically. It has been shown that the induction of potentiation via STDP is less effective at lower frequencies compared to higher frequencies and that depression dominates at lower

frequencies (Sjöström et al., 2001). In addition, EOD production rate for mormyrid fish can vary from a Hz to more than 100 Hz, on average occurring in the ~50-90 Hz range during more active hours, depending on the species, sex, and breeding season (Hopkins, 2009). Although 1 Hz was sufficient to induce synaptic change with focal presynaptic stimulation *in vitro*, 1 Hz is on the lowest end for EOD production rates the fish would experience during an interaction in the wild (Hopkins, 2009). Thus, it would still be very much in the behaviorally relevant range of sensory stimuli to increase the frequency of pairing in electrophysiology experiments or sensory repetition in behavior experiments.

Since I showed that recruitment of more inhibitory pathways likely contributes to the differences of sensory tuning *in vivo*, compared to predictions established *in vitro*, pharmacologically blocking inhibition *in vivo* would be informative. Bath application of a GABA antagonist, like picrotoxin, would block the majority of inhibition across the ELa and ELp. Then doing evoked potential recordings during a sensory pairing or sensory repetition would add more objective evidence for the contributions of inhibition to the non-binary STDP pattern observed *in vivo*.

Additional behavior experiments using a habituation-dishabituation paradigm would also be informative (Carlson et al., 2011). In this experiment, there would still be two sensory stimuli, a conspecific EOD and a 90-degree phase shifted version of the same EOD, as used in Chapter 4. But rather than recording the responses to both EODs at a range of intensities, we would use stimulus trains. Previous work has used stimulus trains of 10 bursts of 10 pulses each, with an intra-burst interval of 30 ms, inter-burst interval of 10 s, and peak-to-peak intensity of 145 mV/cm (Carlson et al., 2011). Bursts 1-8 and burst 10 in the train would be one of the EODs (natural or phase-shifted, randomly decided) and the 9th burst would be the other EOD. EOD rate responses

would be collected from this stimulus train before and after repeating either the natural or shifted EOD. Dishabituation would be measured as the relative difference in EOD rate between the 8th and 9th bursts. For example, recording responses to a shifted EOD train with a natural EOD insert, then repeating the natural EOD, I hypothesize a relatively larger change (9th-8th pulse difference, independent of a relative increase or decrease) to the natural EOD insert after repetition. Rather than the more subtle changes in response I attempted to capture with behavior experiments in Chapter 4, this paradigm may increase the salience of change due to sensory stimulus repetition.

5.4 Conclusion

My dissertation has shown that Hebbian STDP can alter sensory connectivity *in vivo*. I also demonstrated how the same STDP induction dynamics can affect synaptic responses differently *in vivo,* compared to results seen previously *in vitro*. I showed that sensory stimulus repetition alone for the same length of time and rate as previously used for induction of STDP, but without induced postsynaptic spiking, could not alter evoked potential responses or behavioral output. Despite ample evidence for STDP as a mechanism for sensory processing, the work presented in this thesis explores how the mechanics of STDP in sensory tuning *in viv*o cannot be assumed to be the same as discovered *in vitro*. This work can lead to interesting future directions to determine what stimulus dynamics can allow for Hebbian STDP to be clearly induced *in vivo* and for intrinsic network patterns to alter sensory connectivity and behavior.

REFERENCES

Amagai S (1998) Time coding in the midbrain of mormyrid electric fish. II. Stimulus selectivity in the nucleus exterolateralis pars posterior. Journal of Comparative Physiology A: Sensory, Neural, and Behavioral Physiology 182:131–143.

Amagai S, Friedman MA, Hopkins CD (1998) Time coding in the midbrain of mormyrid electric fish. I. Physiology and anatomy of cells in the nucleus exterolateralis pars anterior. Journal of Comparative Physiology A: Sensory, Neural, and Behavioral Physiology 182:115–130.

Arai N, Muller-Dahlhaus F, Murakami T, Bliem B, Lu M-K, Ugawa Y, Ziemann U (2011) State-Dependent and Timing-Dependent Bidirectional Associative Plasticity in the Human SMA-M1 Network. Journal of Neuroscience 31:15376–15383.

Aumentado-Armstrong T, Metzen MG, Sproule MKJ, Chacron MJ (2015) Electrosensory Midbrain Neurons Display Feature Invariant Responses to Natural Communication Stimuli Blackwell KT, ed. PLoS Comput Biol 11:e1004430.

Baker CA, Carlson BA (2014) Short-Term Depression, Temporal Summation, and Onset Inhibition Shape Interval Tuning in Midbrain Neurons. Journal of Neuroscience 34:14272–14287.

Baker CA, Huck KR, Carlson BA (2015) Peripheral sensory coding through oscillatory synchrony in weakly electric fish. eLife 4:e08163.

Baker CA, Kohashi T, Lyons-Warren AM, Ma X, Carlson BA (2013) Multiplexed temporal coding of electric communication signals in mormyrid fishes Krahe R, Fortune E, eds. Journal of Experimental Biology 216:2365–2379.

Baker CA, Ma L, Casareale CR, Carlson BA (2016) Behavioral and Single-Neuron Sensitivity to Millisecond Variations in Temporally Patterned Communication Signals. J Neurosci 36:8985–9000.

Bell C, Grant K (1989) Corollary discharge inhibition and preservation of temporal information in a sensory nucleus of mormyrid electric fish. J Neurosci 9:1029–1044.

Bell CC, Han VZ, Sugawara Y, Grant K (1997) Synaptic plasticity in a cerebellum-like structure depends on temporal order. Nature 387:278–281.

Bi G, Poo M (1998) Synaptic Modifications in Cultured Hippocampal Neurons: Dependence on Spike Timing, Synaptic Strength, and Postsynaptic Cell Type. J Neurosci 18:10464–10472.

Bi G, Poo M (2001) Synaptic Modification by Correlated Activity: Hebb's Postulate Revisited. Annu Rev Neurosci 24:139–166.

Caporale N, Dan Y (2008) Spike Timing–Dependent Plasticity: A Hebbian Learning Rule. Annu Rev Neurosci 31:25–46.

Carlson BA (2002) Electric signaling behavior and the mechanisms of electric organ discharge production in mormyrid fish. Journal of Physiology-Paris 96:405–419.

Carlson BA (2009) Temporal-Pattern Recognition by Single Neurons in a Sensory Pathway Devoted to Social Communication Behavior. Journal of Neuroscience 29:9417–9428.

Carlson BA, Hasan SM, Hollmann M, Miller DB, Harmon LJ, Arnegard ME (2011) Brain Evolution Triggers Increased Diversification of Electric Fishes. Science 332:583–586.

Carlson BA, Hopkins CD (2004) Central control of electric signaling behavior in the mormyrid *Brienomyrus brachyistius* : segregation of behavior-specific inputs and the role of modifiable recurrent inhibition. Journal of Experimental Biology 207:1073–1084.

Carlson BA, Kawasaki M (2008) From stimulus estimation to combination sensitivity: encoding and processing of amplitude and timing information in parallel, convergent sensory pathways. J Comput Neurosci 25:1–24.

Cassenaer S, Laurent G (2007) Hebbian STDP in mushroom bodies facilitates the synchronous flow of olfactory information in locusts. Nature 448:709–713.

Casula EP, Pellicciari MC, Picazio S, Caltagirone C, Koch G (2016) Spike-timing-dependent plasticity in the human dorso-lateral prefrontal cortex. NeuroImage 143:204–213.

Chacron MJ, Doiron B, Maler L, Longtin A, Bastian J (2003) Non-classical receptive field mediates switch in a sensory neuron's frequency tuning. Nature 423:77–81.

Chindemi G et al. (2022) A calcium-based plasticity model for predicting long-term potentiation and depression in the neocortex. Nat Commun 13:3038.

Covey E, Casseday JH (1999) TIMING IN THE AUDITORY SYSTEM OF THE BAT. Annu Rev Physiol 61:457–476.

Dahmen JC, Hartley DEH, King AJ (2008) Stimulus-Timing-Dependent Plasticity of Cortical Frequency Representation. Journal of Neuroscience 28:13629–13639.

Dan Y, Poo M (2004) Spike Timing-Dependent Plasticity of Neural Circuits. Neuron 44:23–30.

Dean I, Harper NS, McAlpine D (2005) Neural population coding of sound level adapts to stimulus statistics. Nat Neurosci 8:1684–1689.

Dempsey C, Abbott L, Sawtell NB (2019) Generalization of learned responses in the mormyrid electrosensory lobe. eLife 8:e44032.

Engert F, Tao HW, Zhang LI, Poo M (2002) Moving visual stimuli rapidly induce direction sensitivity of developing tectal neurons. Nature 419:470–475.

Feldman DE (2000) Timing-Based LTP and LTD at Vertical Inputs to Layer II/III Pyramidal Cells in Rat Barrel Cortex. Neuron 27:45–56.

Feldman DE (2012) The Spike-Timing Dependence of Plasticity. Neuron 75:556–571.

Friedman MA, Hopkins CD (1998) Neural Substrates for Species Recognition in the Time-Coding Electrosensory Pathway of Mormyrid Electric Fish. J Neurosci 18:1171–1185.

Froemke RC (2010) Temporal modulation of spike-timing-dependent plasticity. Front Syna Neurosci Available at: http://journal.frontiersin.org/article/10.3389/fnsyn.2010.00019/abstract [Accessed February 14, 2022].

Froemke RC, Dan Y (2002) Spike-timing-dependent synaptic modification induced by natural spike trains. Nature 416:433–438.

Fujino K, Oertel D (2003) Bidirectional synaptic plasticity in the cerebellum-like mammalian dorsal cochlear nucleus. Proc Natl Acad Sci USA 100:265–270.

George AA, Lyons-Warren AM, Ma X, Carlson BA (2011) A Diversity of Synaptic Filters Are Created by Temporal Summation of Excitation and Inhibition. Journal of Neuroscience 31:14721–14734.

Gooler DM, Feng AS (1992) Temporal coding in the frog auditory midbrain: the influence of duration and rise-fall time on the processing of complex amplitude-modulated stimuli. Journal of Neurophysiology 67:1–22.

Harvey CD, Svoboda K (2007) Locally dynamic synaptic learning rules in pyramidal neuron dendrites. Nature 450:1195–1200.

Hollrigel GS, Ross ST, Soltesz I (1998) Temporal Patterns and Depolarizing Actions of Spontaneous GABA $_A$ Receptor Activation in Granule Cells of the Early Postnatal Dentate Gyrus. Journal of Neurophysiology 80:2340–2351.

Hopkins CD (2009) Electrical Perception and Communication. In: Encyclopedia of Neuroscience, pp 813–831. Elsevier. Available at: https://linkinghub.elsevier.com/retrieve/pii/B9780080450469018271 [Accessed March 20, 2023].

Hopkins CD, Bass AH (1981) Temporal Coding of Species Recognition Signals in An Electric Fish. Science 212:85–87.

Hu B, Wang J-J, Jin C (2020) In vivo odorant input induces spike timing-dependent plasticity of glutamatergic synapses in developing zebrafish olfactory bulb. Biochemical and Biophysical Research Communications 526:532–538.

Huang Q-S, Wei H (2021) A Computational Model of Working Memory Based on Spike-Timing-Dependent Plasticity. Front Comput Neurosci 15:630999.

Jacob V, Brasier DJ, Erchova I, Feldman D, Shulz DE (2007) Spike Timing-Dependent Synaptic Depression in the In Vivo Barrel Cortex of the Rat. Journal of Neuroscience 27:1271–1284.

Kastellakis G, Poirazi P (2019) Synaptic Clustering and Memory Formation. Front Mol Neurosci 12:300.

Kennedy A, Wayne G, Kaifosh P, Alviña K, Abbott LF, Sawtell NB (2014) A temporal basis for predicting the sensory consequences of motor commands in an electric fish. Nat Neurosci 17:416–422.

Kohashi T, Carlson BA (2014) A fast BK-type KCa current acts as a postsynaptic modulator of temporal selectivity for communication signals. Front Cell Neurosci 8 Available at: http://journal.frontiersin.org/article/10.3389/fncel.2014.00286/abstract [Accessed February 14, 2022].

Larkum ME, Nevian T (2008) Synaptic clustering by dendritic signalling mechanisms. Current Opinion in Neurobiology 18:321–331.

Lisman J, Spruston N (2005) Postsynaptic depolarization requirements for LTP and LTD: a critique of spike timing-dependent plasticity. Nat Neurosci 8:839–841.

Lisman J, Spruston N (2010) Questions about STDP as a General Model of Synaptic Plasticity. Front Syn Neurosci 2 Available at: http://journal.frontiersin.org/article/10.3389/fnsyn.2010.00140/abstract [Accessed February 1, 2023].

Lyons-Warren AM, Hollmann M, Carlson BA (2012) Sensory receptor diversity establishes a peripheral population code for stimulus duration at low intensities. Journal of Experimental Biology 215:2586–2600.

Lyons-Warren AM, Kohashi T, Mennerick S, Carlson BA (2013a) Detection of submillisecond spike timing differences based on delay-line anticoincidence detection. Journal of Neurophysiology 110:2295–2311.

Lyons-Warren AM, Kohashi T, Mennerick S, Carlson BA (2013b) Retrograde Fluorescent Labeling Allows for Targeted Extracellular Single-unit Recording from Identified Neurons In vivo. JoVE:3921.

Ma X, Kohashi T, Carlson BA (2013) Extensive excitatory network interactions shape temporal processing of communication signals in a model sensory system. Journal of Neurophysiology 110:456–469.

MacLeod K, Bäcker A, Laurent G (1998) Who reads temporal information contained across synchronized and oscillatory spike trains? Nature 395:693–698.

Markram H, Lübke J, Frotscher M, Sakmann B (1997) Regulation of Synaptic Efficacy by Coincidence of Postsynaptic APs and EPSPs. Science 275:213–215.

Masquelier T, Thorpe SJ (2007) Unsupervised Learning of Visual Features through Spike Timing Dependent Plasticity Friston KJ, ed. PLoS Comput Biol 3:e31.

Mehta MR (2004) Cooperative LTP can map memory sequences on dendritic branches. Trends in Neurosciences 27:69–72.

Mehta MR (2015) From synaptic plasticity to spatial maps and sequence learning: Place Field Plasticity. Hippocampus 25:756–762.

Morrison A, Diesmann M, Gerstner W (2008) Phenomenological models of synaptic plasticity based on spike timing. Biol Cybern 98:459–478.

Mu Y, Poo M (2006) Spike Timing-Dependent LTP/LTD Mediates Visual Experience-Dependent Plasticity in a Developing Retinotectal System. Neuron 50:115–125.

Nelken I (2004) Processing of complex stimuli and natural scenes in the auditory cortex. Current Opinion in Neurobiology 14:474–480.

Richards BA (2010) In vivo spike-timing-dependent plasticity in the optic tectum of Xenopus laevis. Front Syn Neurosci Available at: http://journal.frontiersin.org/article/10.3389/fnsyn.2010.00007/abstract [Accessed March 30, 2022].

Rose G, Fortune E (1996) New techniques for making whole-cell recordings from CNS neurons in vivo. Neuroscience Research 26:89–94.

Schuett S, Bonhoeffer T, Hübener M (2001) Pairing-Induced Changes of Orientation Maps in Cat Visual Cortex. Neuron 32:325–337.

Sharpee TO, Calhoun AJ, Chalasani SH (2014) Information theory of adaptation in neurons, behavior, and mood. Current Opinion in Neurobiology 25:47–53.

Shulz DE (2010) Spike timing dependent plasticity in the intact brain: counteracting spurious spike coincidences. Front Syn Neurosci 4 Available at: http://journal.frontiersin.org/article/10.3389/fnsyn.2010.00137/abstract [Accessed March 13, 2023].

Simoncelli EP, Olshausen BA (2001) Natural Image Statistics and Neural Representation. Annu Rev Neurosci 24:1193–1216.

Singla S, Dempsey C, Warren R, Enikolopov AG, Sawtell NB (2017) A cerebellum-like circuit in the auditory system cancels responses to self-generated sounds. Nat Neurosci 20:943–950.

Sjöström PJ, Turrigiano GG, Nelson SB (2001) Rate, Timing, and Cooperativity Jointly Determine Cortical Synaptic Plasticity. Neuron 32:1149–1164.

Smirnakis SM, Berry MJ, Warland DK, Bialek W, Meister M (1997) Adaptation of retinal processing to image contrast and spatial scale. Nature 386:69–73.

Solomon SG, Kohn A (2014) Moving Sensory Adaptation beyond Suppressive Effects in Single Neurons. Current Biology 24:R1012–R1022.

Song S, Miller KD, Abbott LF (2000) Competitive Hebbian learning through spike-timing-dependent synaptic plasticity. Nat Neurosci 3:919–926.

Taube J, Schwartzkroin P (1988) Mechanisms of long-term potentiation: EPSP/spike dissociation, intradendritic recordings, and glutamate sensitivity. J Neurosci 8:1632–1644.

Testa-Silva G (2010) Human synapses show a wide temporal window for spike-timing-dependent plasticity. Front SynNeurosci Available at: http://journal.frontiersin.org/article/10.3389/fnsyn.2010.00012/abstract [Accessed March 28, 2022].

Tzounopoulos T, Kim Y, Oertel D, Trussell LO (2004) Cell-specific, spike timing–dependent plasticities in the dorsal cochlear nucleus. Nat Neurosci 7:719–725.

Wark B, Lundstrom BN, Fairhall A (2007) Sensory adaptation. Current Opinion in Neurobiology 17:423–429.

Warren R, Sawtell NB (2016) A comparative approach to cerebellar function: insights from electrosensory systems. Current Opinion in Neurobiology 41:31–37.

Whitmire CJ, Stanley GB (2016) Rapid Sensory Adaptation Redux: A Circuit Perspective. Neuron 92:298–315.

Xu-Friedman MA, Hopkins CD (1999) Central mechanisms of temporal analysis in the knollenorgan pathway of mormyrid electric fish. Journal of Experimental Biology 202:1311–1318.

Yao H, Dan Y (2001) Stimulus Timing-Dependent Plasticity in Cortical Processing of Orientation. Neuron 32:315–323.

Yoder N (2022) peakfinder(x0, sel, thresh, extrema, includeEndpoints, interpolate). Available at: (https://www.mathworks.com/matlabcentral/fileexchange/25500-peakfinder-x0-sel-thresh-extrema-includeendpoints-interpolate), [Accessed November 17, 2021].

Zhang LI, Tao HW, Holt CE, Harris WA, Poo M (1998) A critical window for cooperation and competition among developing retinotectal synapses. Nature 395:37–44.